Monthly Notices of the ROYAL ASTRONOMICAL SOCIETY
MNRAS **452,** 1112–1127 (2015) doi:10.1093/mnras/stv1379

Periodic signals from the Circinus region: two new cataclysmic variables and the ultraluminous X-ray source candidate GC X-1

P. Esposito,[1,2]★ G. L. Israel,[3] D. Milisavljevic,[2] M. Mapelli,[4,5] L. Zampieri,[4] L. Sidoli,[1] G. Fabbiano[2] and G. A. Rodríguez Castillo[3]

[1]*INAF–Istituto di Astrofisica Spaziale e Fisica Cosmica – Milano, via E. Bassini 15, I-20133 Milano, Italy*
[2]*Harvard–Smithsonian Center for Astrophysics, 60 Garden Street, Cambridge, MA 02138, USA*
[3]*INAF–Osservatorio Astronomico di Roma, via Frascati 33, I-00040 Monteporzio Catone, Italy*
[4]*INAF–Osservatorio Astronomico di Padova, vicolo dell'Osservatorio 5, I-35122 Padova, Italy*
[5]*INFN, Sezione di Milano Bicocca, piazza della Scienza 3, I-20126 Milano, Italy*

Accepted 2015 June 18. Received 2015 June 9; in original form 2015 May 14

ABSTRACT

The examination of two 2010 *Chandra* ACIS (Advanced CCD Imaging Spectrometer) exposures of the Circinus galaxy resulted in the discovery of two pulsators: CXO J141430.1−651621 and CXOU J141332.9−651756. We also detected 26 ks pulsations in CG X-1, consistently with previous measures. For ∼40 other sources, we obtained limits on periodic modulations. In CXO J141430.1−651621, which is ∼2 arcmin outside the Circinus galaxy, we detected signals at 6120 ± 1 s and 64.2 ± 0.5 ks. In the longest observation, the source showed a flux of $\approx 1.1 \times 10^{-13}$ erg cm^{-2} s^{-1} (absorbed, 0.5–10 keV) and the spectrum could be described by a power law with photon index $\Gamma \simeq 1.4$. From archival observations, we found that the luminosity is variable by ≈50 per cent on time-scales of weeks to years. The two periodicities pin down CXO J141430.1−651621 as a cataclysmic variable of the intermediate polar subtype. The period of CXOU J141332.9−651756 is 6378 ± 3 s. It is located inside the Circinus galaxy, but the low absorption indicates a Galactic foreground object. The flux was $\approx 5 \times 10^{-14}$ erg cm^{-2} s^{-1} in the *Chandra* observations and showed ≈50 per cent variations on weekly/yearly scales; the spectrum is well fitted by a power law with $\Gamma \simeq 0.9$. These characteristics and the large modulation suggest that CXOU J141332.9−651756 is a magnetic cataclysmic variable, probably a polar. For CG X-1, we show that if the source is in the Circinus galaxy, its properties are consistent with a Wolf–Rayet (WR) plus black hole (BH) binary. We consider the implications of this for ultraluminous X-ray sources and the prospects of Advanced LIGO and Virgo. In particular, from the current sample of WR–BH systems, we estimate an upper limit to the detection rate of stellar BH–BH mergers of ∼16 yr^{-1}.

Key words: novae, cataclysmic variables – galaxies: individual: Circinus – X-rays: binaries – X-rays: individual: CG X-1 (CXOU J141312.3−652013) – X-rays: individual: CXOU J141332.9−651756 – X-rays: individual: CXO J141430.1−651621.

1 INTRODUCTION

The *Chandra* ACIS Timing Survey at Brera And Rome astronomical observatories project (CATS @ BAR; Israel et al., in preparation) is a Fourier-transform-based systematic search for new pulsating sources in the *Chandra* Advanced CCD Imaging Spectrometer (ACIS; Garmire et al. 2003) public archive. As of 2015 April 30, 10 282 ACIS timed exposure observations have been examined and ∼457 000 sources were detected. Data taken with gratings or in continuous-clocking mode were not considered. The ∼93 600 light curves of sources with more than 150 photons were searched for coherent signals with an algorithm based on that of Israel & Stella (1996). The limit of 150 counts is related to the intrinsic ability of the Fourier transform to detect a signal with 100 per cent modulation at a minimum confidence level of 3.5σ in 10^5–10^6 trials. CATS @ BAR has so far discovered 43 new certain X-ray pulsators; see Esposito et al. (2013a,b,c) for the first results and Esposito et al. (2014, 2015) for our analogous *Swift* project.

In this paper, we report on the CATS @ BAR results for the galaxy ESO 97-G13 (the 'Circinus galaxy', hereafter CG; Freeman et al. 1977) and its surroundings in the Circinus constellation. CG

★ E-mail: paoloesp@iasf-milano.inaf.it

Table 1. Summary of the X-ray observations used in this work. The hash marks and the star indicate the *Chandra* and *XMM–Newton* observations from which most of the information was obtained.

Satellite	Instrument	Obs. ID	Date	Exp. (ks)	Mode[a]
Chandra	ACIS-23678	355	2000 Jan. 16	1.3	TE FAINT (3.24 s)
Chandra	ACIS-235678	356	2000 Mar. 14	24.7	TE FAINT (3.24 s)
Chandra	ACIS-235678	2454	2001 May 02	4.4	TE FAINT (3.24 s)
*XMM**	pn/MOS 1/MOS 2	0111240101	2001 Aug. 6–7	100.6/104.1/104.0	FF (73.4 ms)/FF (2.6 s)/LW (0.9/2.7 s)
Chandra	ACIS-456789	10873	2009 Mar. 01	18.1	TE HETG VFAINT (2.04 s)
Chandra	ACIS-456789	10850	2009 Mar. 03	13.8	TE HETG VFAINT (2.04 s)
Chandra	ACIS-456789	10872	2009 Mar. 04	16.5	TE HETG VFAINT (2.04 s)
Chandra#	ACIS-23678	12823	2010 Dec. 17–19	154.4	TE VFAINT (3.14 s)
Chandra#	ACIS-23678	12824	2010 Dec. 24	39.4	TE VFAINT (3.14 s)
XMM	pn/MOS 1/MOS 2	0656580601	2014 Mar. 01	32.7/37.8/37.9	FF (73.4 ms)/FF (2.6 s)/LW (2.7 s)

Notes. [a]TE: timed exposure, HETG: high-energy transmission grating, VFAINT: very faint telemetry format, FF: full frame, LW: large window; the readout time is given in parentheses, for the central and peripheral CCDs in the case of the MOS 2 in LW.

is a nearby Seyfert II active galaxy that lies close to the plane of our own Galaxy (J2000 Galactic coordinates: $l = 311.^{\circ}3$, $b = -03.^{\circ}8$; distance $d = 4.2$ Mpc; Tully et al. 2009). The CG contains hydrogen-rich star-forming regions in the inner spiral arms and, due to its closeness, offers a good opportunity to study its population of X-ray sources (Bauer et al. 2001; Sambruna et al. 2001), which includes several ultraluminous X-ray sources (ULXs; Winter, Mushotzky & Reynolds 2006; Mapelli et al. 2010a; Walton et al. 2013; see Mushotzky 2004; Fabbiano 2006; Zampieri & Roberts 2009; Feng & Soria 2011 for reviews on ULXs).

The CG was observed several times with *Chandra*, but it was in two long timed exposure observations carried out in late 2010 that CATS @ BAR pinpointed two new X-ray pulsators in the Circinus region: CXO J141430 and the uncatalogued CXOU J141332. The pipeline detected also CG X-1 (CXOU J141312.3−652013), whose emission is modulated at ∼7 h. CG X-1 is not a new pulsator, but the longstanding debate about its nature (Bauer et al. 2001; Smith & Wilson 2001; Weisskopf et al. 2004) prompted us to include it in our study.

The plan of the paper is as follows. In Section 2, we give details on the X-ray observations used in our study. The rest of the paper is divided into two main parts. The first one focuses on the new pulsators and comprises Sections 3 to 7. In Section 3, we describe the timing analysis that led to the discovery of the new pulsators and allowed us also to set upper limits on the pulsations for dozens of other X-ray sources. The detailed study of CXO J141430 is presented in Section 4 and that of CXOU J141332 in Section 5. To study these sources, we also used data from *XMM–Newton* and optical observations taken with the VLT Survey Telescope (VST). The optical observations and their analysis are described in Section 6. The nature of CXO J141430 and CXOU J141332 is discussed in Section 7.

The second part of the paper is dedicated to CG X-1. In Section 8, we recall the main facts about this source. The results from the analysis of the 2010 *Chandra* data, which were not used before to study CG X-1, are summarized in Section 9. In Section 10, we propose that CG X-1 might be a Wolf–Rayet plus black hole (WR–BH) binary system, and consider the implications of this possibility for ULXs and for the prospects of detection of gravitational radiation from BH–BH mergers. A summary with conclusive remarks follows in Section 11.

2 X-RAY OBSERVATIONS

All the observations used in this work are summarized in Table 1. The most important observations are the ones in which CATS @ BAR detected the new pulsators and its companion, 12823 and 12824, marked with a hash mark in Table 1. They were carried out in a week in 2010 December to study the central region of the CG (Mingo et al. 2012). Their combined exposure is ∼190 ks. In both cases, three ACIS-S and two ACIS-I CCDs were used in full frame mode, ensuring a wide coverage over the Circinus region. The *Chandra* data were processed and analysed with the *Chandra* Interactive Analysis of Observations (CIAO) software package (version 4.7; Fruscione et al. 2006) and the calibration files in CALDB version 4.6.7. The Circinus field as imaged with *Chandra* in observation 12823 is shown in Fig. 1. In the data sets 12823 and 12824, CG X-1 and CXOU J141332 were positioned in the back-illuminated CCD 7 (S3). The photons from these sources were accumulated within a circle with radius 1.5 arcsec and an ellipse with semi-axes 3.5 and 3 arcsec, respectively. CXO J141430 fell on the front-illuminated CCD 3 (I3) and the source counts were extracted from an ellipse with semi-axes of 15 and 14 arcsec. The choice of regions of different sizes is due to the point spread function at the off-axis angles of the sources. For each source, the background was estimated locally, using source-free regions as close as possible to the target. The Solar system barycentre correction to the photon arrival times was applied with AXBARY. The spectra, the redistribution matrices, and the ancillary response files were created using SPECEXTRACT.

The second most useful observation for our study is that performed with *XMM–Newton* in 2001 August with a duration of ∼100 ks (obs. ID 0111240101; Molendi, Bianchi & Matt 2003; it is marked by a star in Table 1). We used the data collected with the European Photon Imaging Camera (EPIC), which consists of two MOS (Turner et al. 2001) and one pn (Strüder et al. 2001) CCD detectors. The raw data were reprocessed using the *XMM–Newton* Science Analysis Software (SAS, version 14.0) and the calibration files in the CCF release of 2015 March. The observation suffered intense soft-proton flares. The intervals of flaring background were located by intensity filters (see e.g. De Luca & Molendi 2004) and excluded from the analysis. This reduced the net exposure time by ∼30 per cent in the pn back-illuminated CCDs and ∼10 per cent in the MOS front-illuminated CCDs. The source photons were extracted from circles with radius of 25 arcsec for CXO J141430

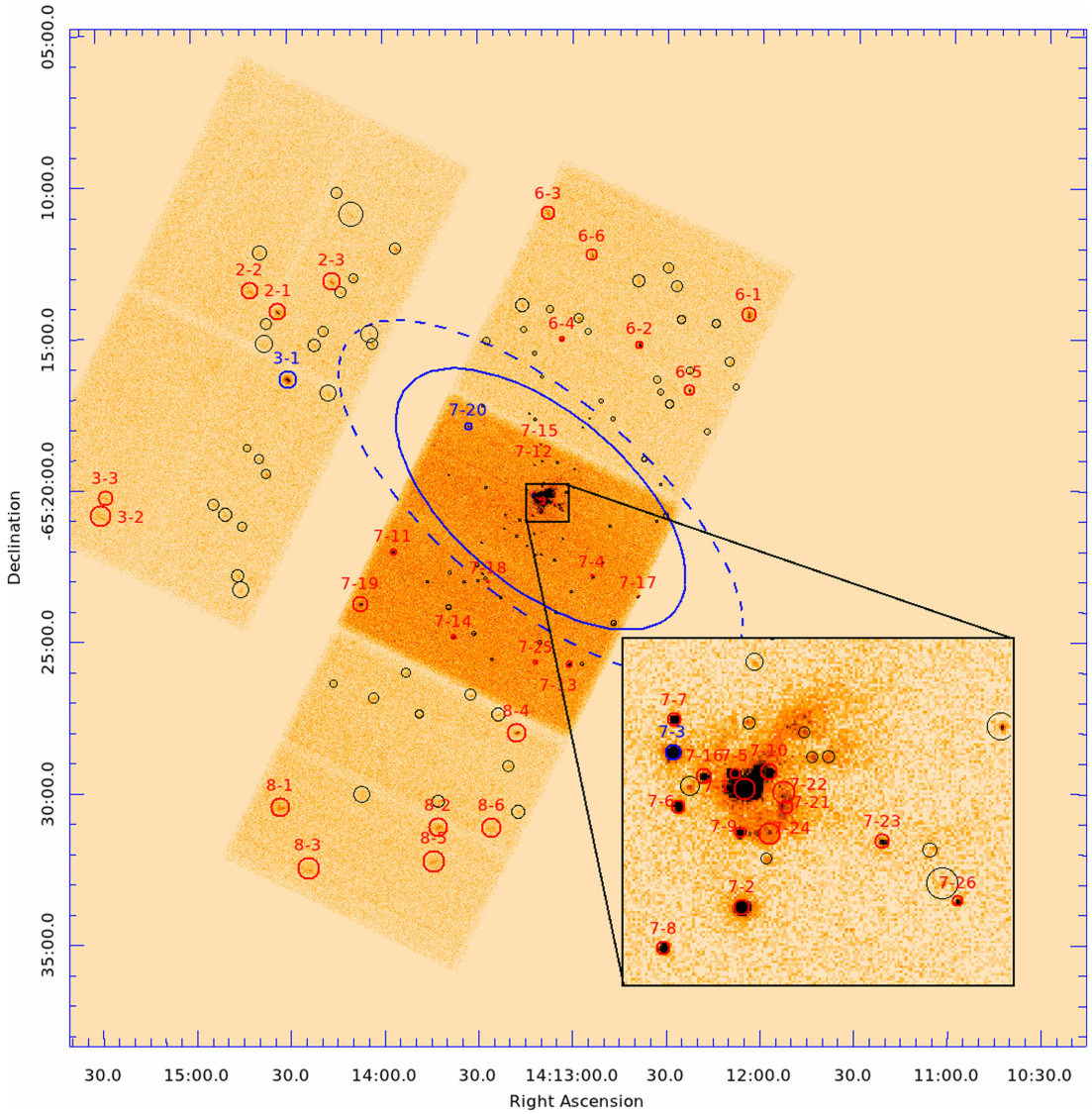

Figure 1. *Chandra*/ACIS image of the Circinus field. North is top and east is left; each CCD subtends an 8.4 arcmin × 8.4 arcmin square on the sky and the zoomed area is 1.2 arcmin × 1 arcmin. Circles mark the detected sources. Red circles indicate sources with >150 counts for which we performed a timing analysis and blue circles the sources from which periodic signals were detected. The labelled sources (with the ACIS CCD number and an identification number) are those for which either signals were detected (source 7–3 is CG X-1, 7–20 is CXOU J141332 and 3–1 is CXO J141430) or an upper limit on the pulsed fraction could be placed (see Fig. 2). The solid and dashed ellipses indicate the size of the CG from 90 per cent total *B* light and total infrared (2MASS) magnitude, respectively (from the NASA/IPAC Extragalactic Database, NED, see http://ned.ipac.caltech.edu/). Source 7–1 is the CG's active galactic nucleus (AGN), 7–2 is the young supernova remnant candidate in the CG (CG X-2; Bauer et al. 2001); other notable sources are the ultraluminous X-ray sources 7–5 = Circinus ULX3, 7–16 = Circinus ULX4, 7–4 = Circinus XMM1 = ULX5, 7–17 = Circinus XMM2 [while Circinus XMM3 is undetected, we used the nomenclature of Winter et al. (2006), Gladstone et al. (2013), and Walton et al. (2013)].

and 15 arcsec for CXOU J141332 (these radii were essentially imposed by CCD gaps and/or the presence of neighbouring sources) and the backgrounds from regions in the same chip as the sources. CXOU J141332 was in the unread part of the central CCD of the MOS 2 operated in a partial window mode, so only pn and MOS 1 data exist for it. Photon arrival times were converted to the Solar system barycentre using the SAS task BARYCEN. The ancillary response files and the spectral redistribution matrices for the spectral analysis were generated with ARFGEN and RMFGEN, respectively. Due to the low number of photons, we combined for each source the spectra from the available EPIC cameras and averaged the response files using EPICSPECCOMBINE.

We made use of other *Chandra* and *XMM–Newton* observations, which were reduced and analysed in a similar way; they provided only detections and flux estimates, or upper limits for the two new pulsators. Six data sets were collected with *Chandra* from 2000 to 2009 with various instrumental setups and durations from ∼1 to 25 ks, and one with *XMM–Newton* in 2014 with exposure of ∼30 ks. Apart from these observations, listed in Table 1, no other *Chandra* pointing of the CG covered the positions of CXO J141430 or

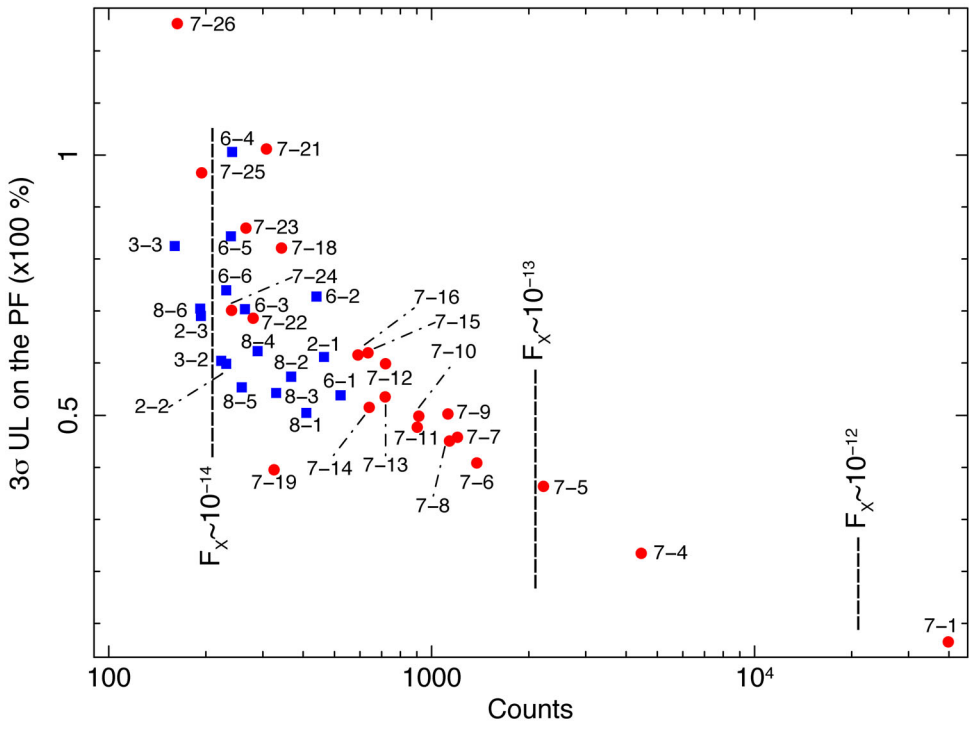

Figure 2. Upper limits on the pulsed fraction of the Circinus sources. Red circles indicate sources detected in the back-illuminated ACIS-7 (S3) CCD and blue squares sources from front-illuminated CCDs. The sources are identified by the same labels as in Fig. 1. Dashed vertical lines mark approximate fluxes for the S3 CCD sources. Source 7–1 is the CG's AGN; other notable sources are: 7–5 = Circinus ULX3, 7–16 = Circinus ULX4, and 7–4 = Circinus XMM1 = ULX5.

CXOU J141332, while in an ∼60 ks observation performed with *XMM–Newton* in 2013 (obs. ID 0701981001), both sources fell either in gaps or at the edge of CCDs, or outside the field of view of the instruments.

3 CATS @ BAR TIMING ANALYSIS

The CIAO WAVEDETECT routine detected 156 sources in the ACIS field of view of observation 12823; they are marked by circles in Fig. 1. The 44 sources with more than 150 photons (those marked by magenta and red circles in Fig. 1) were searched for periodic signals. The CATS @ BAR search algorithm is based on a fast Fourier transform and takes into account also the possible presence of additional non-Poissonian noise components in the Leahy-normalized (Leahy et al. 1983) power spectra (see Israel & Stella 1996 for more details). Correspondingly, the CATS @ BAR signal threshold in a power spectrum, which takes into account the number of independent Fourier frequencies, is also a function of the local underlying noise. For the Circinus data, the maximum frequency of the search (∼0.16 Hz) is dictated by the sampling time of 3.14 s, while the longest period to which the observation is realistically sensitive (because of its duration) is ≈80 ks; 32 768 frequencies were searched. The search resulted in the detection of five sources with significant signals in their power spectra.

In two cases, the power peaks were coincident with the frequencies of known spurious signals due to the spacecraft dithering pattern. The CATS @ BAR pipeline automatically performs check for these artificial signals by means of the CIAO task DITHER_REGION.[1] Furthermore, every candidate signal is cross-checked with the CATS @ BAR data base of recurring signals of instrumental origin, and repeating or dubious signals are carefully inspected and rejected. These two sources are the supernova remnant candidate CG X-2 (Bauer et al. 2001), labelled 7–2 in Fig. 1, and Circinus XMM2, which is classified as an ULX (Winter et al. 2006), labelled 7–17. In a third object, CG X-1, the detected ∼27-ks-period modulation was already known (Bauer et al. 2001; object 7–3 in Fig. 1). This source is discussed in detail in Sections 8–10. The remaining two sources, 3–1 = CXO J141430 (Section 4) and the uncatalogued 7–20 = CXOU J141332 (Section 5), are genuine new X-ray pulsators, as was also confirmed by the other data sets.

For all the other sources with more than 150 events, a 3σ upper limit to the pulsed fraction of any sinusoidal signal was calculated (throughout the paper, we will give 3σ upper limits on non-detections and limits at the 90 per cent confidence level on poorly constrained quantities; all uncertainties will be given at the 1σ confidence level). The pulsed fraction was defined as the semi-amplitude of the sinusoidal modulation divided by the mean count rate. As expected, around 100–200 photons the upper limits start crossing the 100 per cent threshold, above which no meaningful information related to any coherent signal can be inferred. For many other sources, the upper limits are not constraining. For future reference, all the results are summarized in Fig. 2.

4 THE 1.7/17.8 H PULSATOR: CXO J141430

4.1 Timing analysis

CXO J141430 is the brightest of the two new CATS @ BAR pulsators. It shows two distinct periodic signals: an ∼100 per cent modulation at about 6.1 ks and another large-amplitude signal at about 64 ks. The power spectrum is shown in Fig. 3. When the 32 768

[1] See http://cxc.harvard.edu/ciao/ahelp/dither_region.html.

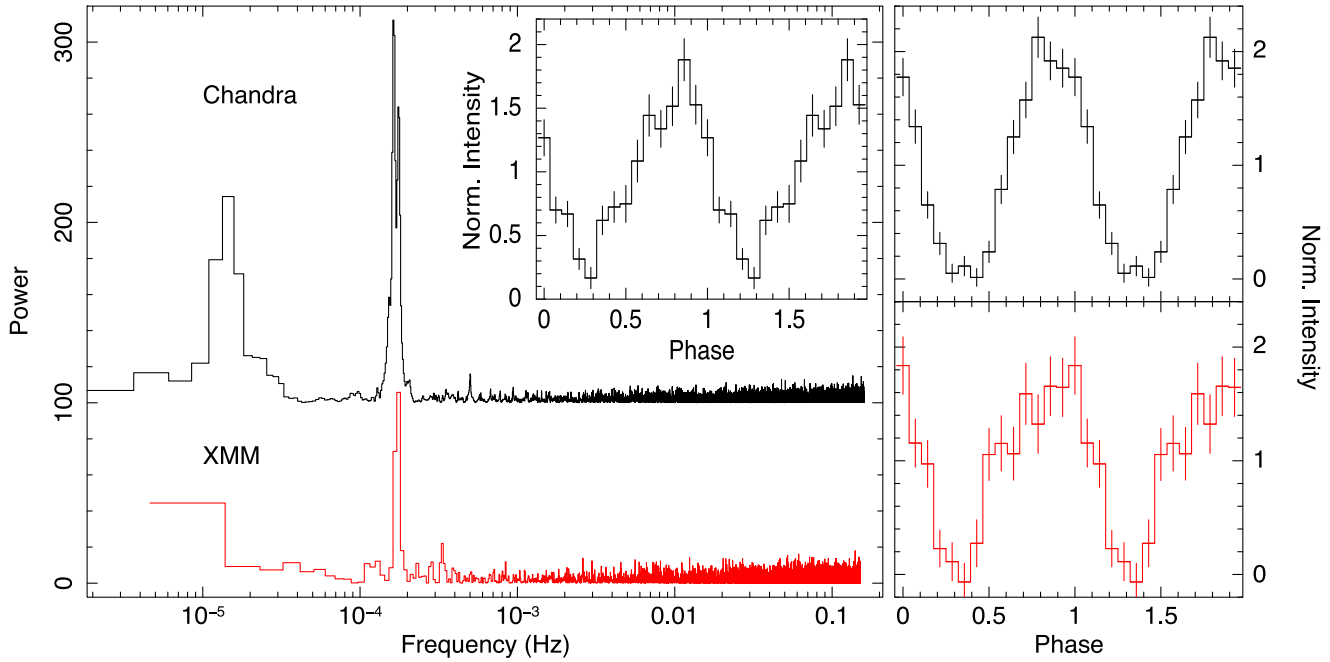

Figure 3. Left-hand panel: 0.5–10 keV power spectra of CXO J141430 obtained from *Chandra*/ACIS (top, black line, observations 12823 and 12824 combined) and *XMM–Newton*/EPIC (bottom, red line) data. For displaying purposes, the *Chandra* data have been shifted in power by +100. The corresponding *Chandra* (top) and *XMM–Newton* (bottom) light curves folded to the best periods are shown in the panels on the right for $P_1 = 6.1$ ks. In the inset is shown the *Chandra* light curve folded to the longer second period $P_2 = 64.2$ ks.

frequencies analysed and the number of sources for which the search was carried out (44) are taken into account, both signals were detected at a confidence level larger than 10σ.

To hone the estimates of the periods, we made use of both the *Chandra* 12823 and 12824 pointings, where about 820 and 250 net counts, respectively, were collected. For the short signal, we used a phase-fitting technique and found $P_1 = 6\,120 \pm 2$ s. For the 64 ks period, the number of sampled cycles, approximately 3, is too small for the phase fitting. We therefore binned the light curve to 6120 s, so to avoid beat-frequency signals produced by the shorter periodicity, and fit a sinusoidal function to it. The fit has a χ^2 of 54 for 30 degrees of freedom (dof) and we derived the period $P_2 = 64.2 \pm 0.5$ ks. The 0.5–10 keV background-subtracted light curves folded on our best periods are shown in Fig. 3. We measured the following pulsed fractions: 100 ± 4 per cent ($P_1 = 6.1$ ks; this value is to be regarded as a lower limit) and 70 ± 4 per cent ($P_2 = 64.2$ ks). Within the statistical uncertainties, the shape and the pulsed fraction of both signals are energy independent. In the soft (<2 keV) and hard (>2 keV) bands, we measured pulsed fractions of 96 ± 5 and 106 ± 5 per cent for the 6.1 ks period, and 69 ± 5 and 64 ± 7 per cent for the 64.2 ks period.

The 6.1 ks signal is significantly detected also in the 2001 *XMM–Newton*/EPIC data (∼700 net counts between the three EPIC cameras), while the observation is too short for the 64.2 ks period (Fig. 3). We measured the period $P_1 = 6.04 \pm 0.04$ ks and a pulsed fraction of 88 ± 12 per cent. CXO J141430 is detected with ∼170 net counts in the 2014 *XMM–Newton* pointing (pn plus MOS 2, in the MOS 1 the source fell in one of the failed CCDs). The short-period pulsations are also clear in that data set, but the low count statistics hampers a precise estimate of the period. Finally, CXO J141430 was in the field of view of *Chandra* also in the observations 355 (2000 January, 1.3 ks) and 356 (2000 March, 25 ks; Table 1). In observation 355, CXO J141430 is detected with a dozen of photons only, and a signal-to-noise ratio SNR $\gtrsim 3$: the short duration and the very small number of photons preclude any analysis of the periodic signals. In the data set 356, the source is detected with about 90 photons (SNR > 9). The 6.1 ks signal can be clearly observed but, similarly than in the 2014 *XMM–Newton* observations, the uncertainty on the period is very large.

4.2 Spectral analysis

For the spectral analysis, we started from the long *Chandra* observation 12823. The fits were performed between 0.6 and 6 keV because of the very low signal of CXO J141430 outside this range. We fit to the data a power-law model, a blackbody, and an optically thin thermal bremsstrahlung. The blackbody model yielded a reduced $\chi^2_\nu = 1.37$ for 40 dof with clearly structured residuals; the derived temperature is $kT = 0.81 \pm 0.03$ keV, while for the absorption there is only an upper limit of $N_{\rm H} < 0.8 \times 10^{22}$ cm^{-2} at 90 per cent confidence. The observed flux was $F_{\rm X} = 6.8^{+0.5}_{-0.4} \times 10^{-14}$ erg cm^{-2} s^{-1} (0.5–10 keV). The power law and the bremsstrahlung gave somewhat better fits, $\chi^2_\nu = 1.27$ and 1.24, respectively, and better residuals. The parameters of the power-law fit (Fig. 4, left) are $N_{\rm H} = 0.36^{+0.14}_{-0.13} \times 10^{22}$ cm^{-2}, $\Gamma = 1.51^{+0.16}_{-0.15}$, and $F_{\rm X} = (1.03 \pm 0.09) \times 10^{-13}$ erg cm^{-2} s^{-1}. For the bremsstrahlung, $N_{\rm H} = 0.31^{+0.11}_{-0.10} \times 10^{22}$ cm^{-2}, $kT = 13^{+12}_{-5}$ keV, and $F_{\rm X} = 0.97^{+0.09}_{-0.10} \times 10^{-13}$ erg cm^{-2} s^{-1}.

In the second *Chandra* observation, the flux was ≈30 per cent higher. The absorption was only poorly constrained (<0.6×10^{22} cm^{-2} at 90 per cent confidence for the power law and <0.5×10^{22} cm^{-2} for the bremsstrahlung), while kT and Γ were consistent with those measured in observation 12823. We thus decided to fit the two spectra simultaneously, with the normalizations free to vary and the other parameters tied up between the data sets. The results are summarized in Table 2.

The 2001 *XMM–Newton* data flatly reject the blackbody model, with $\chi^2_\nu = 2.33$ for 28 dof. The power law provides a good fit to the

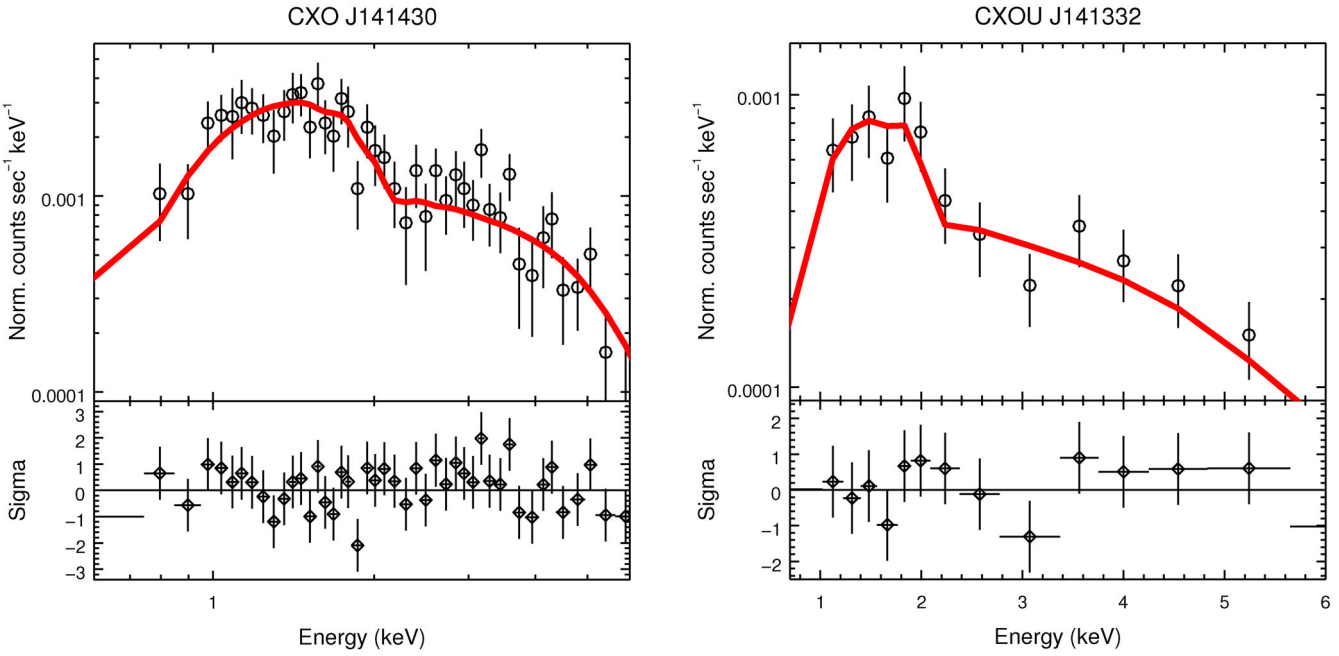

Figure 4. *Chandra*/ACIS spectra and best-fitting power-law models (red solid line) for CXO J141430 and CXOU J141332 (as indicated in each panel) from observation 12823. Bottom panels: residuals in units of standard deviations.

Table 2. Spectral results of CXO J141430. Errors are at a 1σ confidence level for a single parameter of interest.

Model	Data	$N_{\rm H}{}^a$ (10^{22} cm^{-2})	Γ	kT (keV)	Flux^b (10^{-13} erg cm^{-2} s^{-1})	Unabsorbed flux^b	χ^2_ν (dof)
PHABS(POWERLAW)	*Chandra*/12823	$0.30^{+0.13}_{-0.11}$	$1.43^{+0.14}_{-0.13}$	–	1.07 ± 0.08	1.21 ± 0.07	1.12 (52)
	Chandra/12824				$1.40^{+0.15}_{-0.14}$	$1.58^{+0.13}_{-0.12}$	
PHABS(BREMSSTRAHLUNG)	*Chandra*/12823	0.27 ± 0.10	–	18^{+24}_{-7}	$1.01^{+0.10}_{-0.09}$	1.13 ± 0.08	1.10 (52)
	Chandra/12824				$1.32^{+0.16}_{-0.15}$	1.47 ± 0.14	
PHABS(POWERLAW)	*XMM*/0111240101	$<0.3^c$	1.10 ± 0.15	–	0.87 ± 0.08	$0.89^{+0.07}_{-0.06}$	1.02 (28)

Notes. [a]The abundances used are those of Wilms, Allen & McCray (2000); $N_{\rm H}$ values ≈30 per cent lower are derived with those by Anders & Grevesse (1989). The photoelectric absorption cross-sections are from Balucinska-Church & McCammon (1992).
[b]In the 0.5–10 keV energy range.
[c]Upper limit at the 90 per cent confidence level.

data, with an observed flux similar to that of the first *Chandra* observation. The bremsstrahlung fit was equally good. Its temperature, however, could not be constrained, as it always pegged to the highest allowed value, showing that in the *XMM–Newton* data its curvature is indistinguishable from that of a power law. For this reason, in Table 2 we give only the parameters derived from the power-law fit. The quality of the spectrum from the 2014 *XMM–Newton* data is too poor for a spectral analysis. We thus used the models in Table 2 to estimate the flux of CXO J141430, obtaining $F_{\rm X} = (4.8 \pm 0.6) \times 10^{-14}$ erg cm^{-2} s^{-1} for the power-law model and $(3.4 \pm 0.5) \times 10^{-14}$ erg cm^{-2} s^{-1} for the bremsstrahlung. Similarly, for the 2000 *Chandra* observation 356 (∼90 counts in a front-illuminated ACIS-S CCD), we evaluated a flux $F_{\rm X} = (1.1 \pm 0.2) \times 10^{-13}$ erg cm^{-2} s^{-1} for the power-law model and $(8.0 \pm 0.9) \times 10^{-14}$ erg cm^{-2} s^{-1} for the bremsstrahlung. In the short pointing 355, where only a dozen of photons were detected in one of the ACIS-I CCDs, we converted the count rate into a flux with PIMMS[2] and found $F_{\rm X} = (2.0 \pm 0.7) \times 10^{-13}$ erg cm^{-2} s^{-1} for the power-law model and $(1.5 \pm 0.5) \times 10^{-13}$ erg cm^{-2} s^{-1} for the bremsstrahlung.

5 THE 1.8 H PULSATOR: CXOU J141332

5.1 Timing analysis

CXOU J141332 displays a periodicity at roughly 6.4 ks (Fig. 5). This signal was detected at about 3.5σ confidence level in observation 12823 (∼270 counts) and is present also in the shorter pointing

[2] We used the web version of PIMMS (Portable, Interactive Multi-Mission Simulator) available at http://heasarc.gsfc.nasa.gov/cgi-bin/Tools/w3pimms/w3pimms.pl.

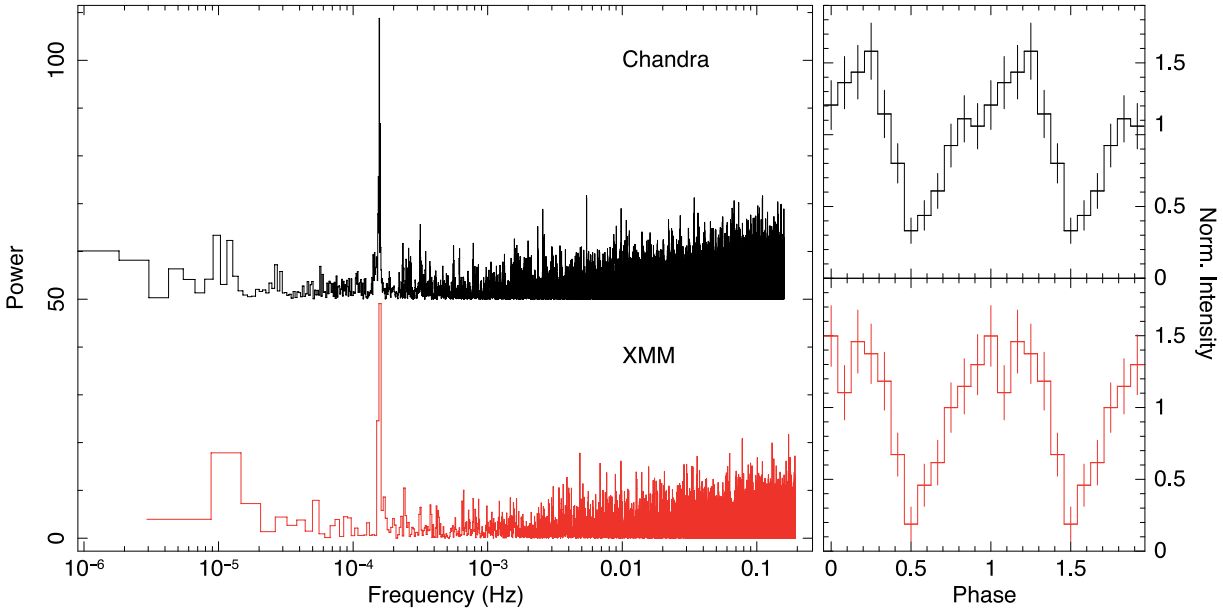

Figure 5. Same as Fig. 3, but for CXOU J141332. For displaying purposes, the *Chandra* data have been shifted in power by +50.

12824 (∼80 counts), though at a lower confidence level. By the phase-fitting analysis, we derived the value $P = 6377 \pm 4$ s. In the corresponding 0.5–10 keV background-subtracted folded profile (Fig. 5), we measured a pulsed fraction of 56 ± 8 per cent. The modulation of CXOU J141332 changes in shape and pulsed fraction as a function of energy: the asymmetry in the profile becomes more accentuated, while the pulsed fraction decreases as the energy increases: 78 ± 7 per cent in the soft range (<2 keV) and 40 ± 8 per cent in the hard range (>2 keV). Of all the other observations in Table 1, CXOU J141332 was detected only in the 2001 *XMM–Newton* data, where the harvest was ∼440 source photons between the pn and MOS 1. We measured a period of 6.4 ± 0.1 ks and the pulsed fraction was 59 ± 10 per cent.

5.2 Spectral analysis

Given the paucity of photons (all in the 1–6 keV range), we performed the spectral analysis by fitting the same spectral models adopted for CXO J141430 to the two *Chandra* data sets 12823 and 12824 simultaneously, with the normalizations free to vary and the other parameters tied up. The blackbody model provides a poor fit to the data, with a $\chi^2_\nu = 1.68$ for 13 dof, while for the bremsstrahlung ($\chi^2_\nu = 1.31$) the temperature could not be constrained. For this reason, in Table 3 we give only the parameters obtained from the power-law fit (see Fig. 4, right), which gave a good fit with a rather hard power law with photon index $\Gamma \approx 0.8$ and a best-fitting absorption $N_{\rm H} = 0.2 \times 10^{22}$ cm^{-2} (with a 90 per cent upper limit of 0.9×10^{22} cm^{-2}). The observed flux was $F_{\rm X} \approx 4 \times 10^{-14}$ erg cm^{-2} s^{-1} during the first observation and $\approx 6 \times 10^{-14}$ erg cm^{-2} s^{-1} in the second; when one considers the large uncertainties, the flux increase is however only marginally significant.

The 2001 *XMM–Newton* observation offers a better spectrum, covering with a few more photons the band 0.4–8 keV. The power-law fit ($\chi^2_\nu = 1.02$ for 16 dof) yielded photon index and flux similar to those derived with *Chandra* (see Table 3) and made it possible to constrain better the absorbing column. This was measured at $N_{\rm H} = 0.13^{+0.09}_{-0.07} \times 10^{22}$ cm^{-2}. In the 2014 *XMM–Newton* observation, CXOU J141332 was not detected. The 3σ upper limit on its observed flux, derived with PIMMS assuming the *XMM–Newton* power-law model in Table 3, was 2×10^{-14} erg cm^{-2} s^{-1} in the 0.5–10 keV band in the MOS data (in the pn, the position of the source occurred in proximity to streaks of out-of-time events due to the nucleus of the CG).

The position of CXOU J141332 was also imaged in the *Chandra* observations 2454, 355, 356, 10850, 10872, and 10873 (see Table 1); the source was never detected and for each data set we derived in a like manner the following upper limits (for the grating observations, we considered only the zero-order data): 1.1×10^{-13} erg cm^{-2} s^{-1} (obs. 355, ACIS-I), 10^{-14} erg cm^{-2} s^{-1} (obs. 356, ACIS-S), 7×10^{-14} erg cm^{-2} s^{-1} (obs. 2454, ACIS-S), 5×10^{-14} erg cm^{-2} s^{-1} (obs. 10873, ACIS-S), 8×10^{-14} erg cm^{-2} s^{-1} (obs. 10850, ACIS-S), and 6×10^{-14} erg cm^{-2} s^{-1} (obs. 10872, ACIS-S).

6 ASTROMETRY AND OPTICAL OBSERVATIONS OF CXO J141430 AND CXOU J141332

6.1 X-ray astrometry

In order to improve the absolute astrometry of the *Chandra* data to search for optical counterparts to CXO J141430 and CXOU J141332, we cross-correlated the X-ray source list obtained using WAVEDETECT with sources in the Two-Micron All-Sky Survey (2MASS; Skrutskie et al. 2006) catalogue, which has an astrometric accuracy better than 0.2 arcsec. We found 17 2MASS point sources coincident within 0.4 arcsec from an X-ray source and used them to register the *Chandra* images on the accurate 2MASS reference frame by fitting a transformation matrix which includes a rotation, scale factor, and translation. We note that the *Chandra*–2MASS superposition did not require a significant transformation: the corrections are of the same order of the residuals (<0.15 arcsec). The resulting positions (J2000.0) of the new CATS @ BAR pulsators are RA = $14^{\rm h}14^{\rm m}30\overset{\rm s}{.}1$ ($\pm 0\overset{\rm s}{.}45$) and Dec. = $-65^\circ 16' 23\overset{''}{.}3$ ($\pm 0\overset{''}{.}30$) for CXO J141430, and RA = $14^{\rm h}13^{\rm m}32\overset{\rm s}{.}9$ ($\pm 0\overset{\rm s}{.}30$) and Dec. = $-65^\circ 17' 56\overset{''}{.}5$ ($\pm 0\overset{''}{.}25$) for CXOU J141332, where the 1σ

Table 3. Spectral results of CXOU J141332. Errors are at a 1σ confidence level for a single parameter of interest.

Model	Data	$N_{\rm H}{}^a$ (10^{22} cm^{-2})	Γ	kT (keV)	Flux^b (10^{-14} erg cm^{-2} s^{-1})	Unabsorbed flux^b	χ^2_ν (dof)
PHABS(POWERLAW)	*Chandra*/12823	$<0.9^c$	$0.8^{+0.3}_{-0.2}$	–	$4.3^{+0.8}_{-0.6}$	$4.5^{+0.6}_{-0.5}$	1.02 (13)
	Chandra/12824				$6.3^{+1.4}_{-1.3}$	$6.5^{+1.2}_{-1.0}$	
PHABS(POWERLAW)	*XMM*/0111240101	$0.13^{+0.09}_{-0.07}$	0.93 ± 0.13	–	5.4 ± 0.5	$5.6^{+0.5}_{-0.4}$	0.82 (16)

Notes. [a]The abundances used are those of Wilms et al. (2000); $N_{\rm H}$ values ≈30 per cent lower are derived with those by Anders & Grevesse (1989). The photoelectric absorption cross-sections are from Balucinska-Church & McCammon (1992).
[b]In the 0.5–10 keV energy range.
[c]Upper limit at the 90 per cent confidence level.

Table 4. VST/OmegaCAM images of regions around CXO J141430 and CXOU J141332.

MJD	Exp. (s)	Filter	Archive name
56442.149	25	r'	OMEGA.2013-05-30T03:34:12.715
56442.156	25	r'	OMEGA.2013-05-30T03:44:47.517
56460.067	25	r'	OMEGA.2013-06-17T01:07:16.243
56460.054	25	r'	OMEGA.2013-06-17T01:18:02.485
56487.025	25	r'	OMEGA.2013-07-14T00:36:46.111
56487.014	40	r'	OMEGA.2013-07-14T00:20:12.159
56488.033	25	r'	OMEGA.2013-07-15T00:47:30.554

uncertainties combine the *Chandra* localization accuracy, the residuals of the *Chandra*–2MASS frame superposition, and the 2MASS absolute astrometric accuracy.

6.2 VST data

Optical images of the regions around CXO J141430 and CXOU J141332 were retrieved from the ESO Science Archive Facility. The observations were originally obtained with the 2.6 m VST located at Paranal Observatory using the OmegaCAM instrument (Kuijken 2011), as part of the VST Photometric Hα Survey of the Southern Galactic Plane and Bulge (Drew et al. 2014). Table 4 lists the details of the images examined.

We aligned and stacked the images using the Image Reduction and Analysis Facility (IRAF) software and the IMALIGN and IMCOMBINE packages following standard procedures. A world coordinate system was then applied using the IMWCS utility[3] and the Third US Naval Observatory CCD Astrograph Catalog (Zacharias et al. 2010). The mean error in the world coordinate system is 0.35 arcsec (3σ) using 22 local stars. We performed aperture photometry on the nearby fields using the IRAF package APPHOT and estimate a limiting magnitude depth of $r' \approx 22.5$ mag. No sources are observed within 2 arcsec of the coordinates of CXO J141430 and CXOU J141332.

7 DISCUSSION I: THE NATURE OF CXO J141430 AND CXOU J141332

With a new X-ray pulsator discovered by CATS @ BAR every ∼2200 light curves, the detection of two previously unknown pulsating sources in the Circinus data set had a formal probability of about 0.04 per cent. While this does not qualify as a statistical anomaly, the 2010 *Chandra* observations have certainly been bountiful for the CATS @ BAR project.

7.1 CXO J141430

In the case of CXO J141430, which is displaced by ∼2 arcmin from the extreme edge of CG (Fig. 1), the two periodicities nail it down as an intermediate polar (IP) with spin period of $P_{\rm spin} = 6.1$ ks (1.7 h) and orbital period $P_{\rm orb} = 64.2$ ks (17.8 h). IPs, also known as DQ Herculis stars, and polars (AM Herculis stars) are the two main subclasses of magnetic cataclysmic variable stars (CVs). CVs are close binaries hosting a white dwarf (WD) accreting from a late-type Roche lobe filling companion, either a main-sequence or a sub-giant star. IPs are characterized by asynchronous rotation ($P_{\rm spin} < P_{\rm orb}$), while polars are phase-locked ($P_{\rm spin} \simeq P_{\rm orb}$) and generally display strong circular polarization (whence the name) at optical and near-infrared wavelengths (see Patterson 1994; Warner 2003; Smith 2006 for reviews). Although it is still matter of debate, these differences are generally interpreted as due to a magnetic field in IPs which is weaker than that typically measured for polars ($B \gtrsim 10^7$ G).

The orbital period of CXO J141430 locates the system above the 2–3 h so-called orbital period gap, where most of the IPs are found. Also the spin-to-orbit period ratio of ∼0.095 is typical of an IP (it is generally in the range 0.25–0.01, with most systems around 0.1).[4] In IPs, the accreted material generally passes through a disc and is then channelled on to the magnetic polar regions of the WD (at variance with polars, where the magnetic field inhibits the formation of the disc). There, a shock develops and the hot gas cools while it settles on to the WD surface emitting X-rays via thermal bremsstrahlung and cyclotron radiation (Aizu 1973). Because of their strong magnetic field, in polars the cooling takes place mainly via cyclotron, whereas IPs are expected to show bremsstrahlung-dominated emission. While the relatively poor statistical quality of the available spectra precluded a good characterization of the X-ray emission of CXO J141430, the results of the spectral analysis are consistent with this picture (Table 2). Also the large-amplitude modulation at the orbital period is rather common in IPs (e.g. Parker, Norton & Mukai 2005), and the ∼100 per cent pulsed fraction hints at a high-inclination system. We finally note that the X-ray luminosity of CXO J141430 in the deep *Chandra* and *XMM–Newton* observations was $L_{\rm X} \approx 2 \times 10^{31} d_1^2$ erg s^{-1} (with a ≈50 per cent variability, see Section 4), where d_1 is the distance in units of 1 kpc. Typical values for IPs, 10^{32}–10^{34} erg s^{-1} (Sazonov et al. 2006), suggest that CXO J141430 is either on the lower side of the luminosity distribution or the distance to the source is substantially larger than ∼1 kpc.

For an IP with orbital period of 17.8 h, a K5V star would be a likely companion (e.g. Smith & Dhillon 1998). Using a value of $N_{\rm H} = 0.3 \times 10^{22}$ cm^{-2} derived from our model fit to the X-ray

[3] See http://tdc-www.harvard.edu/wcstools/.

[4] See for example the catalogue available at the Intermediate Polar Home Page, http://asd.gsfc.nasa.gov/Koji.Mukai/iphome/catalog/members.html.

spectra, and a conversion of $N_{\rm H}/A_V$ of 1.79×10^{21} cm^{-2} mag^{-1} (Predehl & Schmitt 1995), we obtain $A_V = 1.7$ mag. Assuming an absolute magnitude $M_{r'} \approx 7.1$ mag (Bilir et al. 2008),[5] the limiting magnitude $m_{r'} \approx 22.5$ suggests $d > 5$ kpc.

7.2 CXOU J141332

The nature of the fainter CXOU J141332 is less obvious. The source is located inside the 90 per cent total B light contour of the CG. So, the first question that needs to be addressed is whether it is a Galactic or an extragalactic source. Based on the cumulative Galactic X-ray source density versus flux distribution ($\log N$–$\log S$) from the *Chandra* Multi-wavelength Plane survey (ChaMPlane; van den Berg et al. 2012), we estimated the probability of a foreground Galactic object of that flux within this area to be ≈11 per cent. Moreover, its absorbing column measured with *XMM–Newton* ($N_{\rm H} = 1.3^{+0.9}_{-0.7} \times 10^{21}$ cm^{-2}; Table 3) is much lower than the total Galactic value of $\sim 6 \times 10^{21}$ cm^{-2} (Dickey & Lockman 1990; Kalberla et al. 2005). CXOU J141332 is therefore most likely a Galactic source.

The hard X-ray spectrum, a power law with photon index $\Gamma \sim 0.8$–0.9, and the modulation at 6.4 ks (1.8 h) point to a binary system consisting of a compact star accreting from a low-mass companion, where the 1.8 h period likely traces the orbital motion. The period is in fact too long to be the spin of a typical neutron star (NS; with very few possible exceptions; Mattana et al. 2006; Esposito et al. 2011). The low flux and – chiefly – the smooth and ∼60 per cent pulsed-fraction modulation favour a magnetic CV nature also for CXOU J141332 (the period is also too short for the orbit of a standard high-mass X-ray binary). Indeed, CVs are the most abundant population of Galactic compact interacting binaries, and also the most frequent new pulsating sources in the CATS @ BAR sample (Israel et al., in preparation). In particular, since no second periodicity was detected (and lacking any information about optical polarization), the source could be a polar. Polars are generally found at short orbital periods, most of them below the 2–3 h orbital gap, and CXOU J141332 would lie in the peak of their period distribution (e.g. Ritter & Kolb 2003). The profile of the folded light curve (Fig. 5) and its variability as function of energy may indicate a two-pole system. The luminosity during the long 2010 *Chandra* observations was $L_{\rm X} \approx (5$–$8) \times 10^{30} d_1^2$ erg s^{-1}, with the upper limits from the other observations implying a variability of ≈50 per cent or larger. For distances of the order of a few kpc, this is in good agreement with typical values for polars ($L_{\rm X} < 10^{32}$ erg s^{-1}; Sazonov et al. 2006).

For a polar with orbital period of 1.8 h, the companion is likely an M5V star, which has an absolute magnitude of $M_{r'} \approx 12.5$ mag (Bochanski, Hawley & West 2011). The value of $N_{\rm H} = 0.13 \times 10^{22}$ cm^{-2} derived from our model fit to the X-ray spectra implies an $A_V = 0.7$ mag. The limiting magnitude $m_{r'} \approx 22.5$ suggests $d \gtrsim 0.7$ kpc. In the IP hypothesis, assuming for CXOU J141332 a K5V as for CXO J141430, the non-detection would indicate a distance larger than ∼8 kpc.

8 THE CONTROVERSIAL SOURCE CG X-1

CG X-1 (CXOU J141312.3–652013), about 15 arcsec north-east of the Circinus' nucleus, had been known for long to be a bright and variable (possibly periodic) X-ray source. Using high-quality light curves collected with *Chandra*, Bauer et al. (2001) discovered a strong modulation at a period of ∼27 ks. The measured X-ray flux was 9×10^{-13} erg cm^{-2} s^{-1} (0.5–10 keV), and deep *Hubble Space Telescope* (*HST*) observations did not detect any optical counterpart to CG X-1, with a limit $m_{F606W} > 25.3$. They observed that the source might be either a black hole (BH) binary in the CG radiating at $\sim 4 \times 10^{39}$ erg s^{-1} (and hence qualifying as an ULX) or a Galactic CV of the polar type with a particularly long period (in both cases, the 27 ks modulation would reflect the orbital period of the system).

In the polar hypothesis, for an M2V to M6V companion star, the *HST* limit puts the source at a distance larger than 1.2 kpc, implying a luminosity of at least 3×10^{32} erg s^{-1}, a rather extreme value for a polar. Bauer et al. (2001) also noticed that the association of CG X-1 with the CG is convincing: based mainly on the results from the *ASCA* Galactic plane survey (Sugizaki et al. 2001), they evaluated that the possibility of a foreground or background X-ray source is $\lesssim$0.06 per cent. Moreover, Smith & Wilson (2001) noticed that the absorption towards CG X-1 ($N_{\rm H} > 10^{22}$ cm^{-2}) is much larger than the total Galactic column ($N_{\rm H} \sim 6 \times 10^{21}$ cm^{-2}), further supporting the association with the CG. Overall, Bauer et al. (2001), Smith & Wilson (2001), and Bianchi et al. (2002) favoured a very bright extragalactic BH binary, harbouring a BH possibly in excess of 50 $M_\odot$.

Despite recognizing the robustness of the association, Weisskopf et al. (2004) were more open towards the possibility of a foreground polar. They observed that while the period and the luminosity would be somewhat atypical, CG X-1 would be neither the longest period nor the brightest known polar. On the other hand, they argued that if CG X-1 belonged to the CG, because of the short orbital period it should be a BH low-mass X-ray binary (LMXB) with a $\lesssim 1$ $M_\odot$ companion. In this case, the huge X-ray luminosity of the BH would drive the star out of thermal equilibrium and evaporate it within $\sim 10^3$ yr. They regard as very unlikely the possibility that a system this short lived could be observed.

Weisskopf et al. (2004) revised the period of CG X-1 at 26.25 ± 0.15 ks and noticed a possible optical counterpart with $m_{F606W} = 23.5$. However, they did not estimate the significance of the association or of the source, and gave instead a limiting magnitude of 24.3. Ptak et al. (2006) confirmed the limit by Bauer et al. (2001), while a recent work by Gladstone et al. (2013) proposed a counterpart with $m_V = 24 \pm 6$ [presumably, the same excess/source detected by Weisskopf et al. (2004)]. In the literature, CG X-1 is generally considered to be an ULX in the CG (e.g. Bianchi et al. 2002; Swartz et al. 2004; Liu & Mirabel 2005; Ptak et al. 2006; Berghea et al. 2008; Gladstone et al. 2013).

9 THE NEW *CHANDRA* DATA OF CG X-1: ANALYSIS AND RESULTS

Since the CG has been observed many times in X-rays, in particular with *Chandra*, a wealth of data exist for CG X-1. Detailed studies of CG X-1 with *ROSAT*, *BeppoSAX*, *XMM–Newton*, and *Chandra* were presented in the aforementioned works by Smith & Wilson (2001), Bauer et al. (2001), Bianchi et al. (2002), and Weisskopf et al. (2004) (but see also Matt et al. 1996; Guainazzi et al. 1999; Sambruna et al. 2001; Massaro et al. 2006; Bauer et al. 2008; Yang et al. 2009; Shu, Yaqoob & Wang 2011; Walton et al. 2013; Arévalo et al. 2014). A systematic analysis of all the available data is beyond the scope of this paper, and here we will only present results from the analysis of observations 12823/4, which represent the deepest

[5] Uncertainty in the assumed absolute magnitudes of the companion star may be as large as 2 mag. The same holds for CXOU J141332, see below.

and highest quality data set available for this source and, to our knowledge, have not been used so far to study CG X-1.

The coordinates we derived for CG X-1 are RA = $14^{h}13^{m}12\overset{s}{.}24$ ($\pm0\overset{s}{.}25$) and Dec. = $-65^{\circ}20'13\overset{''}{.}82$ ($\pm0\overset{''}{.}25$). Using recent results from the ChaMPlane survey (van den Berg et al. 2012), we confirm the low probability of a foreground or background object ($\lesssim$0.06 per cent) estimated by Bauer et al. (2001). We actually believe that the probability of an interloper is substantially lower (approximately two times smaller), considering that the flux reached by the source in subsequent observations is ∼5 times higher (Weisskopf et al. 2004) and the fact that a background AGN can be excluded by the phenomenology of CG X-1.

For the spectral and timing analysis, we extracted the source counts within a 1.5 arcsec radius, while for the background we used an annulus with radii of 3 and 5 arcsec (see Fig. 1 and Section 2 for more details). The 0.3–8 keV source net count rate was $(6.90 \pm 0.07) \times 10^{-2}$ counts s^{-1} in observation 12823 and $(6.1 \pm 0.1) \times 10^{-2}$ counts s^{-1} in observation 12824. These rates are high enough to cause pileup in the ACIS detector (as we checked with a pileup map). For the spectral analysis, the pileup was dealt with by using the pileup model by Davis (2001). This procedure involves some uncertainty, because the pileup fraction in CG X-1 is strongly dependent on the orbital phase. However, none of our results crucially depends on the exact value of the parameters derived from the spectral fitting.

About six 26 ks cycles were recorded in obs. 12823 and two in obs. 12824. There is a moderate pulse-to-pulse variability, both in shape and in the flux at maximum (≈30 per cent). Also, the average count rate was ≈15 per cent lower during the second observation. To measure the period, we fit a sinusoidal function to the light curve. We obtained $P_{\mathrm{CG\,X-1}} = 26.1 \pm 0.1$ ks. The corresponding folded profile in different energy bands is shown in Fig. 6. The profile is asymmetric and the modulation is large (but the count rate is non-zero also at minimum). The pulsed fraction, defined as[6] $(M - m)/(M + m)$, where M is the maximum count rate and m the minimum, is 91.6 ± 1.5 per cent in the whole band, 89.2 ± 2.5 per cent in the 0.3–2 keV band, and 97.1 ± 1.2 per cent in the 2–8 keV band. A conspicuous spectral softening around minimum is evident from the ratio of the hard to soft counts along the cycle (Fig. 6).

For the spectral analysis, we fit three simple models to the data: a power law, a multicolour disc (MCD; Mitsuda et al. 1984; Makishima et al. 2000), and an optically thin thermal bremsstrahlung, all corrected for the interstellar absorption. While an MCD with $kT \simeq$ 1.3–1.4 keV gives the lowest χ^2, all models provide an acceptable fit to the data (Table 5). All fits confirm that N_{H} towards CG X-1 is substantially larger than the total Galactic absorbing column in that direction. Weisskopf et al. (2004) reported a possible feature, probably a blend of Fe lines, in the 2001 *XMM–Newton* spectrum of CG X-1. No line is required to fit the *Chandra* data (see Fig. 7 for the longest observation); the 3σ upper limit on the equivalent width of any line with central energy between 6 and 7 keV is 0.18 keV in observation 12823. This limit is formally compatible with the equivalent width of 0.23 ± 0.06 keV derived by Weisskopf et al. (2004). However, since there is no trace of such feature in the ACIS data, it is possible that, as noticed also by Weisskopf et al. (2004), the feature observed with *XMM–Newton* is due to residual contamination from the emission of the nuclear region of the CG, which has very strong lines at 6.4 and 7 keV.

[6] Here we adopted a different definition of the pulsed fraction than used before, because the value inferred from a sinusoidal fit would misrepresent the amplitude of the modulation of the 'sawtooth' profile of CG X-1.

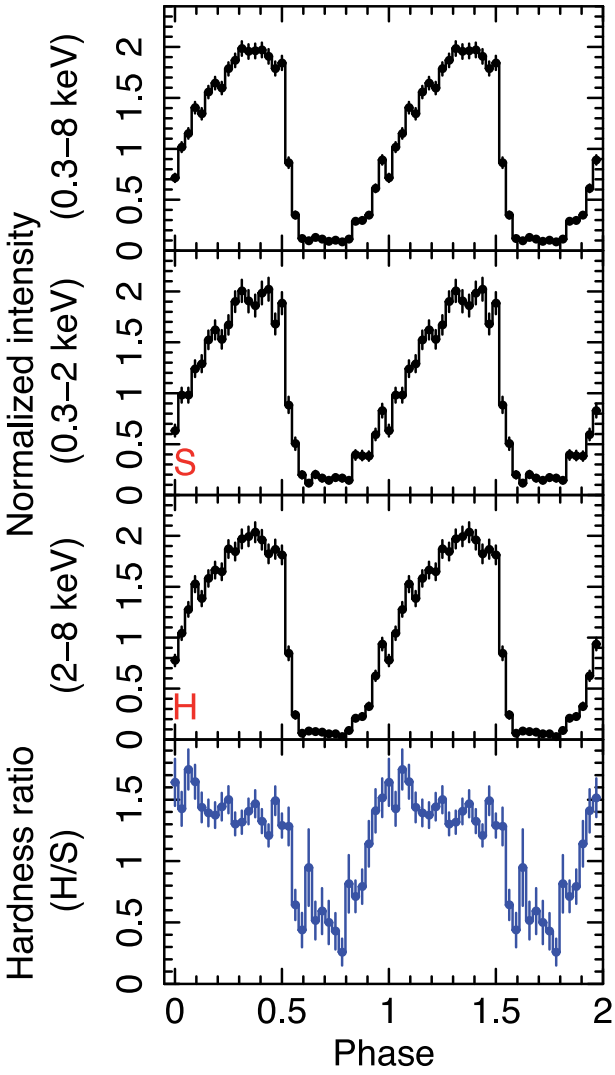

Figure 6. Background-subtracted folded profile of CG X-1 (observation 12823/4) in different energy bands. The hardness ratio between the hard and soft bands is also plotted at the bottom.

We also extracted pulse-resolved spectra from the soft (phase between 0.55 and 0.9 in Fig. 6) and hard (all other phases) parts of the hardness ratio. The data were prepared with DMTCALC, and the spectra of the two data sets from the same phase bins were combined using COMBINE_SPECTRA, which also averaged the response matrices. Although the few counts in the soft spectrum (∼700 versus more than 12 200 in the hard spectrum, after combining the two observations) preclude a detailed comparison, we found that the spectral variation can be described equally well by either a decrease in the absorption during the softening [$N_{\mathrm{H}} = (1.00 \pm 0.03) \times 10^{22}$ cm^{-2} in the hard phase and $(0.24 \pm 0.07) \times 10^{22}$ cm^{-2} in the soft phase for the MCD model; $(1.45 \pm 0.04) \times 10^{22}$ cm^{-2} in the hard phase and $(0.67 \pm 0.08) \times 10^{22}$ cm^{-2} in the soft phase for the power-law model; $(1.29 \pm 0.03) \times 10^{22}$ cm^{-2} in the hard phase and $(0.51 \pm 0.07) \times 10^{22}$ cm^{-2} in the soft phase for the bremsstrahlung model] or a change in the pivotal parameter of the model ($kT = 1.82 \pm 0.05$ keV in the hard phase and 0.95 ± 0.06 keV in the soft phase for the MCD; $\Gamma = 1.70 \pm 0.03$ in the hard phase and 2.54 ± 0.11 in the soft phase for the power law; $kT = 9.4 \pm 0.8$ keV

Table 5. Spectral results of CG X-1. Errors are at a 1σ confidence level for a single parameter of interest.

Model	Obs. ID	$N_{\rm H}{}^a$ (10^{22} cm^{-2})	Γ	kT (keV)	Flux^b (10^{-12} erg cm^{-2} s^{-1})	Unabsorbed flux^b	χ^2_ν (dof)
PHABS(DISKBB)	12823	1.06 ± 0.04	–	1.36 ± 0.07	$0.83^{+0.13}_{-0.12}$	1.17 ± 0.17	0.97 (271)
PHABS(POWERLAW)	12823	1.38 ± 0.05	$1.72^{+0.06}_{-0.05}$	–	$1.23^{+0.10}_{-0.09}$	$1.84^{+0.12}_{-0.10}$	1.04 (271)
PHABS(BREMSSTRAHLUNG)	12823	1.28 ± 0.04	–	$6.5^{+1.0}_{-0.8}$	$1.02^{+0.04}_{-0.05}$	$1.50^{+0.05}_{-0.06}$	1.00 (271)
PHABS(DISKBB)	12824	$1.03^{+0.08}_{-0.07}$	–	$1.33^{+0.14}_{-0.10}$	$0.68^{+0.21}_{-0.16}$	$0.85^{+0.29}_{-0.22}$	0.98 (92)
PHABS(POWERLAW)	12824	$1.38^{+0.11}_{-0.10}$	$1.77^{+0.12}_{-0.10}$	–	$1.00^{+0.15}_{-0.14}$	$1.52^{+0.18}_{-0.17}$	1.11 (92)
PHABS(BREMSSTRAHLUNG)	12824	1.27 ± 0.08	–	$5.6^{+1.7}_{-1.2}$	0.83 ± 0.07	1.25 ± 0.09	1.05 (92)

Notes. [a]The abundances used are those of Wilms et al. (2000); $N_{\rm H}$ values ≈30 per cent lower are derived with those by Anders & Grevesse (1989). The photoelectric absorption cross-sections are from Balucinska-Church & McCammon (1992).
[b]In the 0.5–10 keV energy range.

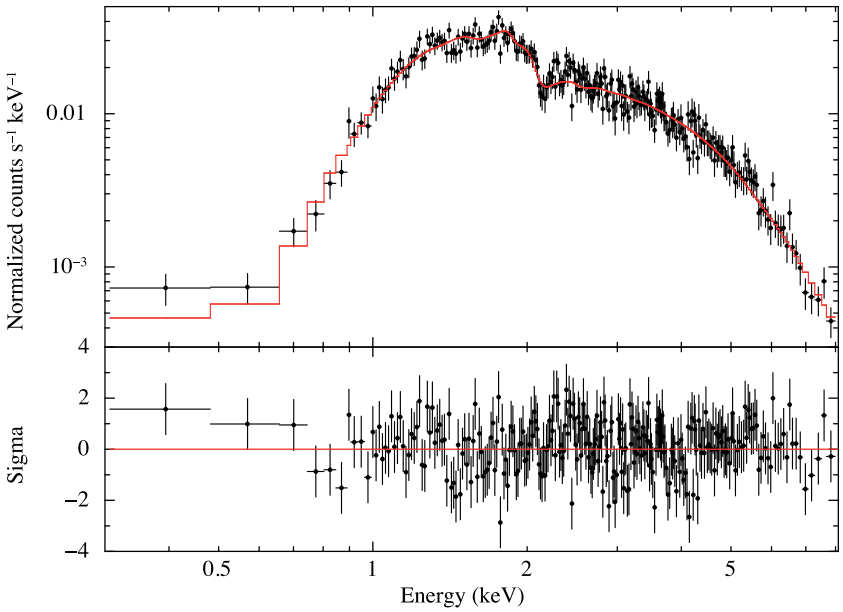

Figure 7. *Chandra*/ACIS spectrum and best-fitting MCD model (red solid line) for CG X-1 from observation 12823. Bottom panel: the residuals of the fit in units of standard deviations.

in the hard phase and 2.4 ± 0.3 keV in the soft phase for the bremsstrahlung).

10 DISCUSSION II: IS CG X-1 A WOLF–RAYET/BH BINARY IN THE CG?

While we cannot completely exclude the chance superposition of a Galactic polar in the direction of the inner part of the CG, we regard the association of the CG X-1 to the CG as rather compelling. In the following, we will discuss the nature of the source in this framework.

Weisskopf et al. (2004) disfavoured the possibility of a BH LMXB because such a system would be rather short lived, and thus unlikely to be observed. This argument is not conclusive when dealing with an individual source (one can be lucky enough to observe a rare system!), but we too deem an LMXB as unlikely. This is because of its orbital profile (Fig. 6). In fact, most LMXBs show no or very low amplitude modulation on their orbital period. In those which display orbital modulation, dipping and/or eclipsing systems, the morphology of the profile is very different. In dipping systems, the dips are produced by absorption of X-rays due to accreting matter located in the bulge at the outer edge of the accretion disc (e.g. Díaz Trigo et al. 2006); the X-ray minima tend to be rather sharp and to show a harder-than-average emission, which is the opposite of what is observed in CG X-1 (Fig. 6, bottom panel). LMXB eclipses display sharp and abrupt ingresses and egresses, due to the small size of the X-ray-emitting regions. Even the smoothly modulated accretion disc corona sources (systems viewed nearly edge-on where the outer edge of the dense disc modulates the X-rays from the central source scattered into the line of sight by an extended ionized corona; Mason & Cordova 1982; White & Holt 1982; Somero et al. 2012) have different profiles. Moreover, LMXBs containing BHs are usually transient X-ray sources, with outburst durations of the order of weeks to months (e.g. Remillard & McClintock 2006), while CG X-1 is variable but persistent.

On the other hand, the light curve and the folded profile of CG X-1 bear a strong resemblance to those observed in high-mass X-ray binaries (HMXBs) with a Wolf–Rayet (WR) star companion: Cyg X-3 in the Milky Way ($P = 4.8$ h; Zdziarski et al. 2012), IC 10 X-1 in IC 10 ($P = 35$ h; Prestwich et al. 2007), NGC 300 X-1 in NGC 300 ($P = 33$ h; Carpano et al. 2007b), and the candidates CXOU J123030.3+413853 in NGC 4490 (CXOU J123030; $P = 6.4$ h; Esposito et al. 2013c) and CXOU J004732.0−251722.1 in NGC 253 (with a candidate periodicity $P \sim 14$–15 h; Maccarone

et al. 2014).[7] The large modulation of these systems, showing a slow rise and a faster decay, is different from what observed in almost any other class of X-ray sources [see, e.g., the arguments summarized in Esposito et al. (2013c) about the source in NGC 4490], and can be considered the signature of WR HMXBs.

Although its properties remain still poorly understood, the best studied source of this kind is Cyg X-3, where the orbital modulation has been ascribed to attenuation by electron scattering in the strong WR wind (Hertz, Joss & Rappaport 1978). A further significant contribution to the scattering medium is thought to be a bulge of ionized matter formed by the collision of the stellar wind with the outer accretion disc (Zdziarski, Misra & Gierliński 2010). Alternative explanations involve orbital modulation by absorbers in different phases (hot/ionized and cold/clumpy, triggered by the BH jet bow shock; Vilhu & Hannikainen 2013), or the presence of the accretion wake, a large-scale asymmetry around the compact object (Okazaki & Russell 2014). The orbital profile of CG X-1 is even more asymmetric than in Cyg X-3, probably due to rather extreme properties of the absorbing/scattering medium or because of a higher inclination of the system. The variation of the hardness ratio along the orbit (Fig. 6), showing a clear softening during the X-ray minimum, could be due to direct X-rays almost completely blocked by dense matter (probably the innermost regions of the WR wind when the X-ray source is at the superior conjunction). The softer X-rays observed could be due to down-scattering into the line of sight of central X-rays by cold and less dense material located farther away from the WR star (similarly to what usually observed during eclipses in some HMXBs; Haberl 1991).

Weisskopf et al. (2004) mentioned for CG X-1 the possibility of a WR or, more in general, a naked He donor, but did not discuss it in detail owing to the scarcity of information of such systems. In particular, they observed that for an $\sim$2 $M_\odot$ companion, their argument against LMXB systems was still relevant. However, thanks to their compactness, even more massive WR stars can comfortably fit in the orbit of a system like CG X-1 (the stellar radius of a 20 $M_\odot$ WR star is <2 $R_\odot$; e.g. Langer 1989; Schaerer & Maeder 1992). Also the other main observational properties of CG X-1 fit well in the scenario of a WR–BH HMXB in the CG.[8]

If one considers the reddening towards the CG (4 mag) and its distance module (28.1 mag, from NED), the limit on the optical counterpart by Bauer et al. (2001) and Ptak et al. (2006) implies $M_V > -6.8$. This value is compatible with a WR star, for which M_V is typically in the range from -2.5 to -7 (e.g. Massey 2003).

The X-ray luminosity of CG X-1 is variable by a factor of $\approx$10 (Bianchi et al. 2002; Weisskopf et al. 2004). The highest flux reported in the literature (5.2×10^{-12} erg cm^{-2} s^{-1} for a power-law fit or 5×10^{-12} erg cm^{-2} s^{-1} for an MCD fit, in the 0.5–8 keV band; Weisskopf et al. 2004) would imply, for a distance of 4.2 Mpc, a 0.5–10 keV luminosity of $L_X = (1.5\text{–}2) \times 10^{40}$ erg s^{-1}. If the system is Eddington-limited, the lower limit on the mass of the accreting BH is $M_{BH} \gtrsim 75$ $M_\odot$ for an He or C/O donor. For the system to shine in X-rays, the velocity of the WR star wind has to be slow enough to allow the formation of an accretion disc. This condition corresponds for CG X-1 to the requirement $M_{BH} \gtrsim 1.5\, v^4_{w,1000}\delta^2$ $M_\odot$, where M_{BH} is the BH mass, $v_{w,1000}$ is the wind velocity in units of 1000 km s^{-1}, and $\delta \approx 1$ is a dimensionless parameter (adapted from Carpano et al. 2007b, see also Illarionov & Sunyaev 1975). In the simplest wind-accretion case (e.g. Edgar 2004), the luminosity can be estimated as

$$L_X \approx \eta \frac{\dot{M}_w c^2 G^2 M^2_{BH}}{a^2 (v^2_{orb} + v^2_w)^2}, \quad (1)$$

where η is the efficiency, $\dot{M}_w$ is the wind mass-loss rate, a is the orbital separation, v_{orb} is the orbital velocity, and v_w is the wind velocity at the BH orbit. Assuming $\dot{M}_w = 10^{-5}$ $M_\odot$ yr^{-1} and $v_w = 1000$ km s^{-1} for the WR star (e.g. Crowther 2007), $a = 5.8 \times 10^{11}$ cm (for a 10 $M_\odot$ companion), $M_{BH} = 75$ $M_\odot$, and the formation of a disc with $\eta = 0.1$, the corresponding luminosity is $L_X \simeq 2 \times 10^{40}$ erg s^{-1}. More in general, for $M_{BH} > 10$ $M_\odot$ and all the other things being equal, one finds $L_X \gtrsim 3 \times 10^{39}$ erg s^{-1}. In case of Roche lobe overflow, even higher X-ray luminosity could be achieved. However, we note that if CG X-1 is indeed a WR–BH binary, the WR star is probably not filling its Roche lobe [unless it is very massive; see for example the discussion of the case of Cyg X-3, where the orbital period is much shorter, in Szostek & Zdziarski (2008)]. An X-ray luminosity of $\sim 2 \times 10^{40}$ erg s^{-1} can be therefore accounted for. We finally notice that, although we do not regard the question as crucial, the problem of the lifetime of the system discussed by Weisskopf et al. (2004) would be significantly attenuated, since the WR phase of a massive O-type star is thought to last a few $\times 10^5$ yr (Meynet & Maeder 2005).

10.1 Statistics, environment, and WR–BH binaries as ULXs

All known WR HMXBs have been mentioned in the previous section. Three have been established so far as certain WR–BH systems: IC 10 X-1, NGC 300 X-1, and M101 ULX-1. For the fourth WR–compact object binary, Cyg X-3 in our Galaxy, it is still debated whether the compact object is a BH or an NS. There are however several pieces of evidence (radio, infrared, and X-ray emission properties) that point to a 2–5 $M_\odot$ BH, as suggested also by evolutionary models (e.g. Lommen et al. 2005; Szostek & Zdziarski 2008; Szostek, Zdziarski & McCollough 2008; Shrader, Titarchuk & Shaposhnikov 2010; Zdziarski, Mikołajewska & Belczyński 2013). Apart from CG X-1, discussed in this paper, two additional WR–BH binary candidates were found in the last two years: CXOU J123030 in NGC 4490 and CXOU J004732.0−251722.1 in NGC 253.

We expect WR–BH binaries to be associated with star-forming regions, since WR are young stars with massive progenitors (with zero-age main-sequence mass $\gtrsim$25 $M_\odot$). Table 6 shows the star formation rate (SFR) of the host galaxies of WR–BH binaries and binary candidates. The average SFR is $\sim$2 $M_\odot$ yr^{-1}, which is quite high for nearby late-type galaxies. All metallicities listed in Table 6 are sub-solar. Recent *N*-body and population synthesis simulations of young star clusters (Mapelli et al. 2013; Mapelli & Zampieri 2014) suggest that $\approx$2 per cent of all HMXBs powered by BHs in star-forming regions are BH–WR binaries, independent of star cluster metallicity.

The average luminosity of CG X-1 in the *Chandra* observations presented here makes it a bona fide ULX. The maximum luminosity reached by the source, following Weisskopf et al. (2004), is $L_X = (1.5\text{–}2) \times 10^{40}$ erg s^{-1}. At such flux levels, in high counting statistics *XMM–Newton* spectra, a persistent ULX typically shows the hallmark of the ultraluminous state (Gladstone, Roberts & Done 2009), with the presence of two thermal components, one of which

[7] Apart from these objects, the only other known WR HMXB is ULX-1 in M101 (Liu et al. 2013, see also Section 10.1). A period of 8.2 d was inferred from radial velocities of optical emission lines, but no X-ray light curves of good quality are available for this source.

[8] Even bright ($L_X > 10^{40}$ erg s^{-1}) ULXs may contain an NS (King 2009; Bachetti et al. 2014), although such systems are probably not the majority (Fragos et al. 2015). Here, we will not discuss this possibility.

Table 6. Properties of observed WR–BH binaries and candidates (denoted by stars), and of their host galaxies.

Host galaxy	Source	Period (h)	BH mass[a] ($M_\odot$)	WR mass[a] ($M_\odot$)	SFR[b] ($M_\odot$ yr^{-1})	Z[b] ($Z_\odot$)	t_{GW}[c] (Gyr)
IC 10	X-1	34.9	33	35	0.07	0.22	1.4
NGC 300	X-1	32.8	20	26	0.14	0.19	1.7
NGC 4490	CXOU J123030.3+413853*	6.4	–	–	4.5	0.23	0.038
NGC 253	CXOU J004732.0−251722.1*	14.5	–	–	4.0	0.24	0.33
Circinus	CG X-1*	7.2	–	–	1.5	0.10	0.052
M101	ULX-1	196.8	20	19	3.1	0.17	200
Milky Way	Cyg X-3	4.8	3	7	0.25	0.31	0.051

[a]For the BH and WR masses, we list only the fiducial values that we use to derive the merger rates R in equation (2). Most of these masses are very uncertain, as discussed in Prestwich et al. (2007), Silverman & Filippenko (2008), Carpano et al. (2007a,b), Crowther et al. (2010), Esposito et al. (2013c), Maccarone et al. (2014), Liu et al. (2013), and Shrader et al. (2010).
[b]The values of SFR and metallicity of the host galaxy come from the compilation of Mapelli et al. (2010a). The metallicity Z refers to the value at $0.7R_{25}$, where R_{25} is the Holmberg radius of the galaxy, for NGC 253, NGC 300, NGC 4490, M101, and for the Milky Way, while it is the total metallicity for IC 10 and Circinus. We assume $Z_\odot = 0.02$.
[c]The parameter t_{GW} is the time-scale for the binary to coalesce, under the assumptions discussed in the main text.

centred at rather soft energies (∼0.1–0.2 keV) and the other producing a shallow but significant rollover around 3–5 keV. Such a spectrum is usually interpreted as the imprint of a super-Eddington accretion regime (e.g. Middleton, Sutton & Roberts 2011).

As discussed in Section 8, the X-ray spectrum of the *Chandra* observations considered here is satisfactorily fit with a single-component model. The lack of evidence of multiple components may be real, but may also be caused by the comparatively low statistics (the flux is ∼5 times lower than at maximum) and/or by the fact that *Chandra* has a lower sensitivity than *XMM–Newton* below ∼0.5 keV, where the soft component peaks. If the spectrum is intrinsically single component, this may suggest that CG X-1 does not enter into the ultraluminous state and hence does not accrete above Eddington.

The latter possibility is consistent with the scenario discussed above in which accretion proceeds through a wind and the accretion rate does not exceed the Eddington limit. For wind accretion from a compact WR star, the very formation of a standard accretion disc is uncertain and the accretion efficiency can in general be smaller than that of a standard disc (e.g. Frank, King & Raine 2002). A scenario of rather efficient accretion from a wind of a massive WR star on to a BH of a few tens $M_\odot$ has been invoked also for M101 ULX-1. This source is a WR–BH ULX system with a dynamical mass measurement and a cool disc X-ray spectrum at maximum (Liu et al. 2013), and it has a significantly larger orbital period (∼8 d, see Table 6) and smaller luminosity (∼3×10^{39} erg s^{-1}) than CG X-1. Assuming a similar scenario also for CG X-1, simple BH mass estimates based on Eddington-limited accretion from an He–WR star (as those reported above) give $M_{BH} \gtrsim 70\ M_\odot$ for the observed maximum luminosity. Such a massive BH would populate the high-mass tail of the distribution of BHs formed through direct collapse of a massive star in a low-metallicity environment (Mapelli, Colpi & Zampieri 2009; Zampieri & Roberts 2009; Belczynski et al. 2010), a scenario indeed consistent with the metallicity inferred for the CG (see Table 6). In the same hypothesis, an independent limit can be obtained from the normalization of the disc component at maximum luminosity (*Chandra* Obs. ID 365; Weisskopf et al. 2004), giving $M_{BH} \simeq 8[(d/4.2\,\mathrm{Mpc})/\sqrt{\cos i}]\ M_\odot$ (i is the inclination angle of the disc; e.g. Lorenzin & Zampieri 2009).

On the other hand, the lack of a high counting statistics spectrum at maximum luminosity prevents us from reaching a robust conclusion. We thus briefly consider also the possibility that the system is accreting from a particularly massive and big WR companion via Roche lobe overflow, for which the mass transfer rate is expected to significantly exceed the Eddington limit (e.g. Lommen et al. 2005). In this assumption, the maximum observed luminosity of CG X-1 would place it in the populated part of the ULX luminosity distribution (e.g. Swartz et al. 2011), where the observed flux can be produced by moderately beamed, super-Eddington emission from accretion on to a BH of a few tens $M_\odot$ (or even a canonical stellar-mass BH).

It is interesting to compare the properties of the two candidate WR–BH ULX systems that we have tentatively identified, CG X-1 and CXOU J123030 in NGC 4490 (Esposito et al. 2013c). While the orbital periods are similar (7.2 and 6.4 h, respectively), the X-ray luminosity is significantly different (CG X-1 being >10 times more luminous). Assuming a similar scenario of sub-Eddington accretion from a wind with the formation of a disc, the different luminosity could be mostly ascribed to the different BH mass, with CG X-1 being about ∼10 times more massive than CXOU J123030. For non-extreme inclinations, this is consistent with the BH mass inferred from the normalization of the disc component of CXOU J123030, for which we obtained $M_{BH} \simeq 2.8[(d/8\,\mathrm{Mpc})/\sqrt{\cos i}]\ M_\odot$ (Esposito et al. 2013c). On the other hand, in case of non-standard super-Eddington accretion via Roche lobe overflow, the larger luminosity of CG X-1 may be caused by the larger accretion rate and we would then be witnessing the different X-ray outcome produced by similar BHs in very different accretion environments.

10.2 WR–BH binaries as precursors of BH–BH binaries

There is great uncertainty on the expected rate of BH–BH mergers in the frequency range that will be observed by Advanced LIGO and Virgo (∼10–10^4 Hz; Abadie et al. 2010). In fact, while for NS–NS binaries the expected merger rate can be derived from the properties of the observed NS–NS binaries (e.g. Kim, Kalogera & Lorimer 2003) and from the rate of short gamma-ray bursts (e.g. Coward et al. 2012; Fong et al. 2012), no evidence has been found of BH–BH systems yet. WR–BH binaries can provide us with essential clues, since they are a possible precursor of BH–BH binaries (or BH–NS binaries), provided that the system is so tight that it remains bound when the WR star evolves into a compact remnant.

Here, we use the properties of all known WR–BH binaries and candidates to infer the BH–BH merger rate in the instrumental range

of Advanced LIGO and Virgo. The main source of uncertainty is represented by the fate of the WR: we do not know the natal kick and the mass of the compact remnant that will form from the evolution of the WR. In particular, the natal kick might unbind the binary or transform it into a loose system that will not merge in a Hubble time. Thus, population synthesis simulations of the evolution of each WR–BH system are necessary, in order to predict the binary fate (e.g. Belczynski et al. 2013). On the other hand, our knowledge of the current orbital parameters and of the masses of the binary members is poor for most WR–BH systems: the WR star has been detected only in Cyg X-3, IC 10 X-1, NGC 300 X-1, and M101 ULX-1, and the mass of the BH is poorly determined even in these four cases, due to the uncertainty on the inclination and because the WR winds might affect the radial velocity estimate (e.g. Maccarone et al. 2014; Laycock, Maccarone & Christodoulou 2015). Given these uncertainties, population synthesis models can hardly constrain the fate of most WR–BH candidates. Thus, we adopt a much simpler approach in order to obtain an upper limit to the BH–BH merger rate from the observed WR–BH binaries and candidates. As already done by Maccarone et al. (2014), we assume that all seven WR–BH candidates in our sample will become BH–BH binaries through direct collapse of the WR star (leading to a secondary BH mass $m_2 = 10\ \mathrm{M}_\odot$), and that the orbital properties of the binary will be substantially unchanged after the collapse of the WR star. When even the mass of the primary BH is not known (Table 6), we assume $m_1 = 10\ \mathrm{M}_\odot$.

Thus, the rate of BH–BH mergers per Mpc^3 (R) can be approximately estimated as (see e.g. Mapelli et al. 2010b, 2012; Ziosi et al. 2014)

$$R = \rho_{\mathrm{SFR}}(z) \sum_i (t_{\mathrm{GW,\,i}} + t_{\mathrm{evol,\,i}})^{-1}\,(\mathrm{SFR}_i)^{-1}, \qquad (2)$$

where $\rho_{\mathrm{SFR}}(z)$ is the cosmic SFR density (Hopkins & Beacom 2006), $t_{\mathrm{GW,i}}$ is the coalescence time-scale of the ith binary ($i = 1, \ldots, 7$ in our sample, see Table 6), $t_{\mathrm{evol,\,i}}$ is the time elapsed from the formation of the ith binary (as a binary of two main-sequence stars) to the birth of the second BH, and SFR_i is the current SFR of the ith galaxy. For our sample, we assume $t_{\mathrm{evol\,i}} \approx 3 \times 10^6$ yr, which is the main-sequence lifetime of the most massive stars. The values of SFR_i are from Table 6. Equation (2) gives a strong upper limit for the sample, for the fact that we neglect local galaxies that do not host any WR–BH binary.

The coalescence time-scale t_{GW} can be expressed as (Peters 1964)

$$t_{\mathrm{GW}} = \frac{5}{256}\,\frac{c^5\,a^4\,(1-e^2)^{7/2}}{G^3\,m_1\,m_2\,(m_1+m_2)}, \qquad (3)$$

where c is the light speed, G is the gravitational constant, a is the semi-major axis and e is the eccentricity of the orbit. We assume $e = 0$ for all considered binaries. Table 6 shows the values of t_{GW} for each considered binary, under these assumptions. The value of t_{GW} for M101 ULX-1 is much larger than the Hubble time: the impact of this system is negligible for any estimate of the Advanced LIGO and Virgo detection rate. The second longest value of t_{GW} is $\sim$2 Gyr (for NGC 300 X-1): this value is well below the Hubble time, and implies that we might detect at present time the merger of systems like NGC 300 X-1 that formed $\sim$2 Gyr ago, i.e. at redshift $z = 0.3$, when the SFR density was a factor of 2 higher than now [$\rho_{\mathrm{SFR}}(z = 0.3) \sim 3.6 \times 10^{-2}\ \mathrm{M}_\odot\ \mathrm{yr}^{-1}\ \mathrm{Mpc}^{-3}$; Hopkins & Beacom 2006]. To obtain the best favourable upper limit, we use $\rho_{\mathrm{SFR}}(z = 0.3) = 3.6 \times 10^{-2}\ \mathrm{M}_\odot\ \mathrm{yr}^{-1}\ \mathrm{Mpc}^{-3}$ for all sources in equation (2), and we obtain $R \sim 4 \times 10^{-9}$ and $1 \times 10^{-9}\ \mathrm{yr}^{-1}\ \mathrm{Mpc}^{-3}$, if we include or do not include Cyg X-3 among the WR–BH candidates, respectively. Since Advanced LIGO and Virgo will detect BH–BH mergers out to $\sim$1 Gpc, we can infer upper limits to the detection rate of BH–BH mergers of $\sim$16 and 5 events per year, if we include or do not include Cyg X-3, respectively. Such rates are consistent with those predicted in previous papers that study WR–BH binaries (e.g. Belczynski et al. 2013; Maccarone et al. 2014). It is worth noting that our upper limit is quite close to the 'pessimistic' estimate of the BH–BH merger rate by the Advanced LIGO–Virgo collaboration (whose pessimistic and optimistic rates are $R = 10^{-10}$ and $3 \times 10^{-7}\ \mathrm{yr}^{-1}\ \mathrm{Mpc}^{-3}$, respectively; Abadie et al. 2010).

11 SUMMARY AND CONCLUSIONS

We reported on our timing survey of the deep *Chandra*/ACIS observations of the CG and its surroundings (Fig. 1). Approximately 150 X-ray sources were detected and for about 40 of them, enough photons were collected to search for periodic signals by means of a Fourier transform. We discovered two new X-ray pulsators, CXO J141430 and the uncatalogued CXOU J141332, and bumped into the already known periodic modulation of the notable and controversial source CG X-1 ($P \simeq 7.2$ h; Bauer et al. 2001). For the other sources, we set upper limits on the presence of periodic signals (Fig. 2).

CXO J141430 is more than 2 arcmin out of the border of the CG. A spin period of 1.7 h and an orbital period of 17.8 h give the source away as an IP seen at large inclination. Its X-ray spectrum can be modelled by a power law with photon index $\Gamma \simeq 1.4$. The flux in the longest *Chandra* observation was $\approx 1 \times 10^{-13}$ erg $\mathrm{cm}^{-2}\ \mathrm{s}^{-1}$ and other observations imply a variability of $\approx$50 per cent on time-scales of weeks to years. The typical luminosity of IPs and the non-detection of the optical counterpart suggest a distance larger than $\sim$5 kpc.

Albeit at $\sim$3.5 arcmin from the nucleus, CXOU J141332 appears inside the CG. However, the low absorption column, which is much smaller than the total Galactic density, argues against an extragalactic source. Indeed, the probability of a foreground Galactic X-ray source is substantial ($\approx$10 per cent). The period of this source is 1.8 h and the spectrum is hard: it can be described by a power law with $\Gamma \simeq 0.9$. The observed flux was $\approx 5 \times 10^{-14}$ erg $\mathrm{cm}^{-2}\ \mathrm{s}^{-1}$, with $\approx$50 per cent variations on weekly/yearly scales. We believe that also CXOU J141332 is a Galactic magnetic CV, most probably of the polar type. Assuming that the companion is an M5V star (or similar), the non-detection of its optical counterpart is not particularly constraining for the distance, implying only $d \gtrsim 0.7$ kpc. On the other hand, if the system is within a few kpc, its luminosity is in the normal range for polars.

We deem the association of CG X-1 with the CG convincing. Prompted by the similarity of its modulation to the distinctive ones of the known WR HMXBs and candidates, we advanced the possibility that CG X-1 might be one of such systems. The observations of CG X-1 (in particular, the high luminosity implied and the limits on the optical counterpart) are consistent with this hypothesis. The dearth of observed WR HMXBs is puzzling, since they should be relatively common and very bright (Lommen et al. 2005; Linden, Valsecchi & Kalogera 2012). Though there is no obvious bias against their detection, it is possible that some of these objects might be misclassified or unrecognized. At any rate, in the last few years, the sample of WR HMXBs has grown rapidly to four confirmed sources and three candidates (including CG X-1), all of them outside our Galaxy, with the exception of Cyg X-3. Besides their relevance for the population of X-ray binaries and ULXs, WR–BH

systems are very important as they might be progenitors of double-BH systems. We used the information from the current sample of systems to estimate an upper limit to the detection rate of stellar BH–BH mergers with Advanced LIGO and Virgo, which turned out to be $\sim$16 yr^{-1} for a distance range of 1 Gpc.

ACKNOWLEDGEMENTS

This research is based on data obtained from the *Chandra* Data Archive and has made use of software provided by the *Chandra* X-ray Center (CXC) in the application package CIAO and SHERPA. This research has also made use of data obtained from the ESA's *XMM–Newton* Science Archive (XSA) and from the ESO Science Archive Facility (under request number 161735), and of the NED, which is operated by the JPL, Caltech, under contract with the NASA. The IRAF software is distributed by the NOAO, which is operated by AURA, Inc., under cooperative agreement with the NSF. PE acknowledges a Fulbright Research Scholar grant administered by the US–Italy Fulbright Commission and is grateful to the Harvard–Smithsonian Center for Astrophysics for hosting him during his Fulbright exchange. MM acknowledges financial support from the MIUR through grant FIRB 2012 RBFR12PM1F, and from INAF through grants PRIN-2011-1 and PRIN-2014-14. LZ acknowledges financial support from the ASI/INAF contract no. I/037/12/0. LS acknowledges the PRIN-INAF 2014 grant 'Towards a unified picture of accretion in High Mass X-Ray Binaries'. PE thanks M. Mezcua for surveying the available *HST* data of the Circinus region and A. Wolter for comments on the manuscript.

REFERENCES

Abadie J. et al., 2010, Class. Quantum Grav., 27, 173001
Aizu K., 1973, Prog. Theor. Phys., 49, 1184
Anders E., Grevesse N., 1989, Geochim. Cosmochim. Acta, 53, 197
Arévalo P. et al., 2014, ApJ, 791, 81
Bachetti M. et al., 2014, Nature, 514, 202
Balucinska-Church M., McCammon D., 1992, ApJ, 400, 699
Bauer F. E., Brandt W. N., Sambruna R. M., Chartas G., Garmire G. P., Kaspi S., Netzer H., 2001, AJ, 122, 182
Bauer F. E., Dwarkadas V. V., Brandt W. N., Immler S., Smartt S., Bartel N., Bietenholz M. F., 2008, ApJ, 688, 1210
Belczynski K., Bulik T., Fryer C. L., Ruiter A., Valsecchi F., Vink J. S., Hurley J. R., 2010, ApJ, 714, 1217
Belczynski K., Bulik T., Mandel I., Sathyaprakash B. S., Zdziarski A. A., Mikołajewska J., 2013, ApJ, 764, 96
Berghea C. T., Weaver K. A., Colbert E. J. M., Roberts T. P., 2008, ApJ, 687, 471
Bianchi S., Matt G., Fiore F., Fabian A. C., Iwasawa K., Nicastro F., 2002, A&A, 396, 793
Bilir S., Karaali S., Ak S., Yaz E., Cabrera-Lavers A., Coşkunoğlu K. B., 2008, MNRAS, 390, 1569
Bochanski J. J., Hawley S. L., West A. A., 2011, AJ, 141, 98
Carpano S., Pollock A. M. T., Wilms J., Ehle M., Schirmer M., 2007a, A&A, 461, L9
Carpano S., Pollock A. M. T., Prestwich A., Crowther P., Wilms J., Yungelson L., Ehle M., 2007b, A&A, 466, L17
Coward D. M. et al., 2012, MNRAS, 425, 2668
Crowther P. A., 2007, ARA&A, 45, 177
Crowther P. A., Barnard R., Carpano S., Clark J. S., Dhillon V. S., Pollock A. M. T., 2010, MNRAS, 403, L41
Davis J. E., 2001, ApJ, 562, 575
De Luca A., Molendi S., 2004, A&A, 419, 837
Díaz Trigo M., Parmar A. N., Boirin L., Méndez M., Kaastra J. S., 2006, A&A, 445, 179
Dickey J. M., Lockman F. J., 1990, ARA&A, 28, 215
Drew J. E. et al., 2014, MNRAS, 440, 2036
Edgar R., 2004, New Astron. Rev., 48, 843
Esposito P., Turolla R., De Luca A., Israel G. L., Possenti A., Burrows D. N., 2011, MNRAS, 418, 170
Esposito P., Israel G. L., Sidoli L., Mason E., Rodríguez Castillo G. A., Halpern J. P., Moretti A., Götz D., 2013a, MNRAS, 433, 2028
Esposito P., Israel G. L., Sidoli L., Rodríguez Castillo G. A., Masetti N., D'Avanzo P., Campana S., 2013b, MNRAS, 433, 3464
Esposito P., Israel G. L., Sidoli L., Mapelli M., Zampieri L., Motta S. E., 2013c, MNRAS, 436, 3380
Esposito P., Israel G. L., Sidoli L., Tiengo A., Campana S., Moretti A., 2014, MNRAS, 441, 1126
Esposito P. et al., 2015, MNRAS, 450, 1705
Fabbiano G., 2006, ARA&A, 44, 323
Feng H., Soria R., 2011, New Astron. Rev., 55, 166
Fong W. et al., 2012, ApJ, 756, 189
Fragos T., Linden T., Kalogera V., Sklias P., 2015, ApJ, 802, L5
Frank J., King A., Raine D. J., 2002, Accretion Power in Astrophysics, 3rd edn. Cambridge Univ. Press, Cambridge, UK
Freeman K. C., Karlsson B., Lynga G., Burrell J. F., van Woerden H., Goss W. M., Mebold U., 1977, A&A, 55, 445
Fruscione A. et al., 2006, in Silva D. R., Doxsey R. E., eds, Proc. SPIE Conf. Ser. Vol. 6270, Observatory Operations: Strategies, Processes, and Systems. SPIE, Bellingham, p. 62701V
Garmire G. P., Bautz M. W., Ford P. G., Nousek J. A., Ricker G. R., Jr 2003, in Truemper J. E., Tananbaum H. D., eds, Proc. SPIE Conf. Ser. Vol. 4851, X-Ray and Gamma-Ray Telescopes and Instruments for Astronomy. SPIE, Bellingham, p. 28
Gladstone J. C., Roberts T. P., Done C., 2009, MNRAS, 397, 1836
Gladstone J. C., Copperwheat C., Heinke C. O., Roberts T. P., Cartwright T. F., Levan A. J., Goad M. R., 2013, ApJS, 206, 14
Guainazzi M. et al., 1999, MNRAS, 310, 10
Haberl F., 1991, A&A, 252, 272
Hertz P., Joss P. C., Rappaport S., 1978, ApJ, 224, 614
Hopkins A. M., Beacom J. F., 2006, ApJ, 651, 142
Illarionov A. F., Sunyaev R. A., 1975, A&A, 39, 185
Israel G. L., Stella L., 1996, ApJ, 468, 369
Kalberla P. M. W., Burton W. B., Hartmann D., Arnal E. M., Bajaja E., Morras R., Pöppel W. G. L., 2005, A&A, 440, 775
Kim C., Kalogera V., Lorimer D. R., 2003, ApJ, 584, 985
King A. R., 2009, MNRAS, 393, L41
Kuijken K., 2011, The Messenger, 146, 8
Langer N., 1989, A&A, 210, 93
Laycock S. G. T., Maccarone T. J., Christodoulou D. M., 2015, MNRAS, preprint (arXiv:1506.03882)
Leahy D. A., Darbro W., Elsner R. F., Weisskopf M. C., Kahn S., Sutherland P. G., Grindlay J. E., 1983, ApJ, 266, 160
Linden T., Valsecchi F., Kalogera V., 2012, ApJ, 748, 114
Liu Q. Z., Mirabel I. F., 2005, A&A, 429, 1125
Liu J.-F., Bregman J. N., Bai Y., Justham S., Crowther P., 2013, Nature, 503, 500
Lommen D., Yungelson L., van den Heuvel E., Nelemans G., Portegies Zwart S., 2005, A&A, 443, 231
Lorenzin A., Zampieri L., 2009, MNRAS, 394, 1588
Maccarone T. J., Lehmer B. D., Leyder J. C., Antoniou V., Hornschemeier A., Ptak A., Wik D., Zezas A., 2014, MNRAS, 439, 3064
Makishima K. et al., 2000, ApJ, 535, 632
Mapelli M., Zampieri L., 2014, ApJ, 794, 7
Mapelli M., Colpi M., Zampieri L., 2009, MNRAS, 395, L71
Mapelli M., Ripamonti E., Zampieri L., Colpi M., Bressan A., 2010a, MNRAS, 408, 234
Mapelli M., Huwyler C., Mayer L., Jetzer P., Vecchio A., 2010b, ApJ, 719, 987
Mapelli M., Ripamonti E., Vecchio A., Graham A. W., Gualandris A., 2012, A&A, 542, A102
Mapelli M., Zampieri L., Ripamonti E., Bressan A., 2013, MNRAS, 429, 2298

Mason K. O., Cordova F. A., 1982, ApJ, 262, 253
Massaro F., Bianchi S., Matt G., D'Onofrio E., Nicastro F., 2006, A&A, 455, 153
Massey P., 2003, ARA&A, 41, 15
Matt G. et al., 1996, MNRAS, 281, L69
Mattana F., Götz D., Falanga M., Senziani F., de Luca A., Esposito P., Caraveo P. A., 2006, A&A, 460, L1
Meynet G., Maeder A., 2005, A&A, 429, 581
Middleton M. J., Sutton A. D., Roberts T. P., 2011, MNRAS, 417, 464
Mingo B., Hardcastle M. J., Croston J. H., Evans D. A., Kharb P., Kraft R. P., Lenc E., 2012, ApJ, 758, 95
Mitsuda K. et al., 1984, PASJ, 36, 741
Molendi S., Bianchi S., Matt G., 2003, MNRAS, 343, L1
Mushotzky R., 2004, Prog. Theor. Phys. Suppl., 155, 27
Okazaki A. T., Russell C. M. P., 2014, in Ishida M., Petre R., Mitsuda K., eds, Suzaku-MAXI 2014: Expanding the Frontiers of the X-ray Universe, p. 202
Parker T. L., Norton A. J., Mukai K., 2005, A&A, 439, 213
Patterson J., 1994, PASP, 106, 209
Peters P. C., 1964, Phys. Rev., 136, 1224
Predehl P., Schmitt J. H. M. M., 1995, A&A, 293, 889
Prestwich A. H. et al., 2007, ApJ, 669, L21
Ptak A., Colbert E., van der Marel R. P., Roye E., Heckman T., Towne B., 2006, ApJS, 166, 154
Remillard R. A., McClintock J. E., 2006, ARA&A, 44, 49
Ritter H., Kolb U., 2003, A&A, 404, 301
Sambruna R. M., Brandt W. N., Chartas G., Netzer H., Kaspi S., Garmire G. P., Nousek J. A., Weaver K. A., 2001, ApJ, 546, L9
Sazonov S., Revnivtsev M., Gilfanov M., Churazov E., Sunyaev R., 2006, A&A, 450, 117
Schaerer D., Maeder A., 1992, A&A, 263, 129
Shrader C. R., Titarchuk L., Shaposhnikov N., 2010, ApJ, 718, 488
Shu X. W., Yaqoob T., Wang J. X., 2011, ApJ, 738, 147
Silverman J. M., Filippenko A. V., 2008, ApJ, 678, L17
Skrutskie M. F. et al., 2006, AJ, 131, 1163
Smith R. C., 2006, Contemp. Phys., 47, 363
Smith D. A., Dhillon V. S., 1998, MNRAS, 301, 767
Smith D. A., Wilson A. S., 2001, ApJ, 557, 180
Somero A., Hakala P., Muhli P., Charles P., Vilhu O., 2012, A&A, 539, A111
Strüder L. et al., 2001, A&A, 365, L18
Sugizaki M., Mitsuda K., Kaneda H., Matsuzaki K., Yamauchi S., Koyama K., 2001, ApJS, 134, 77
Swartz D. A., Ghosh K. K., Tennant A. F., Wu K., 2004, ApJS, 154, 519
Swartz D. A., Soria R., Tennant A. F., Yukita M., 2011, ApJ, 741, 49
Szostek A., Zdziarski A. A., 2008, MNRAS, 386, 593
Szostek A., Zdziarski A. A., McCollough M. L., 2008, MNRAS, 388, 1001
Tully R. B., Rizzi L., Shaya E. J., Courtois H. M., Makarov D. I., Jacobs B. A., 2009, AJ, 138, 323
Turner M. J. L. et al., 2001, A&A, 365, L27
van den Berg M., Penner K., Hong J., Grindlay J. E., Zhao P., Laycock S., Servillat M., 2012, ApJ, 748, 31
Vilhu O., Hannikainen D. C., 2013, A&A, 550, A48
Walton D. J. et al., 2013, ApJ, 779, 148
Warner B., 2003, Cataclysmic Variable Stars. Cambridge Univ. Press, Cambridge, UK
Weisskopf M. C., Wu K., Tennant A. F., Swartz D. A., Ghosh K. K., 2004, ApJ, 605, 360
White N. E., Holt S. S., 1982, ApJ, 257, 318
Wilms J., Allen A., McCray R., 2000, ApJ, 542, 914
Winter L. M., Mushotzky R. F., Reynolds C. S., 2006, ApJ, 649, 730
Yang Y., Wilson A. S., Matt G., Terashima Y., Greenhill L. J., 2009, ApJ, 691, 131
Zacharias N. et al., 2010, AJ, 139, 2184
Zampieri L., Roberts T. P., 2009, MNRAS, 400, 677
Zdziarski A. A., Misra R., Gierliński M., 2010, MNRAS, 402, 767
Zdziarski A. A., Maitra C., Frankowski A., Skinner G. K., Misra R., 2012, MNRAS, 426, 1031
Zdziarski A. A., Mikołajewska J., Belczyński K., 2013, MNRAS, 429, L104
Ziosi B. M., Mapelli M., Branchesi M., Tormen G., 2014, MNRAS, 441, 3703

This paper has been typeset from a TEX/LATEX file prepared by the author.